frontiers | Frontiers in Earth Science

TYPE Original Research
PUBLISHED 17 June 2024
DOI 10.3389/feart.2024.1389378

OPEN ACCESS

EDITED BY
Reza Barati,
University of Kansas, United States

REVIEWED BY
Wendong Wang,
China University of Petroleum (East China), China
Hongjian Zhu,
Yanshan University, China
Kim Sarah Mews,
Norwegian University of Science and Technology, Norway

*CORRESPONDENCE
Delei Shang,
sdl18@tsinghua.org.cn

RECEIVED 21 February 2024
ACCEPTED 22 May 2024
PUBLISHED 17 June 2024

CITATION
Liu G, Shang D, Zhao Y and Du X (2024), Characterization of brittleness index of gas shale and its influence on favorable block exploitation in southwest China.
Front. Earth Sci. 12:1389378.
doi: 10.3389/feart.2024.1389378

Characterization of brittleness index of gas shale and its influence on favorable block exploitation in southwest China

Guojun Liu[1,2], Delei Shang [3]*, Yuan Zhao[4,5] and Xidong Du[6]

[1]Hunan Engineering Research Center of Structural Safety and Disaster Prevention for Urban Underground Infrastructure, College of Civil Engineering, Hunan City University, Yiyang, China, [2]State Key Laboratory of Coal Mine Disaster Dynamics and Control, Chongqing University, Chongqing, China, [3]State Key Laboratory of Intelligent Construction and Healthy Operation and Maintenance of Deep Underground Engineering, Guangdong Provincial Key Laboratory of Deep Earth Sciences and Geothermal Energy Exploitation and Utilization, Institute of Deep Earth Sciences and Green Energy, College of Civil and Transportation Engineering, Shenzhen University, Shenzhen, China, [4]Sinohydro Bureau 8 Co., Ltd., POWERCHINA, Changsha, China, [5]Department of Hydraulic Engineering, Tsinghua University, Beijing, China, [6]Faculty of Land Resources Engineering, Kunming University of Science and Technology, Kunming, China

The microstructure, mineral composition, total organic carbon content, etc., of gas shale are crucial parameters for shale reservoirs, which can directly/indirectly affect shale brittleness, fracturing effect, adsorption ability and production efficiency. The study proposed a workflow to characterize the physical and mechanical parameters of Lower Silurian Longmaxi shale outcrop samples extracted from the favorable block in Changning, Sichuan, southwest China. This study elaborated on the influence of these physical and mechanical characteristics and proposed a corresponding brittleness index on shale extraction. In addition, it put forward corresponding suggestions for development and risk control. For a better understanding the mechanisms of shale gas storage and production, XRD, XRF, SEM, low temperature Nitrogen adsorption method, nuclear magnetic resonance and other measurements were employed to analyze and study the mineral composition, microstructure, and adsorption performance of shale. The results demonstrated that the pores of shale are mainly slit pores; there are diverse pore types in shale, mainly including intergranular pores, mineral particle dissolution pores, and internal pores of organic matter; The samples with relatively low porosity also noticeably exhibit ultra-low permeability, and the nanopore structure is remarkably significant, with distribution primarily in range of 5–237 nm. Finally, a brittleness index considering the influence of water content and the mechanical properties was proposed, and the coupling interaction of various minerals components and mechanical properties on the brittleness index can more objectively reflect the brittleness characteristics of deep shale formation.

KEYWORDS

shale gas, microstructure, brittleness index, porous medium, fracability, hydraulic fracturing

Highlights

- Focusing on advantages and exploiting significance of shale gas favorable block in southwest China
- Obtained and characterized firsthand basic physical and mechanical parameters of Longmaxi shale
- Proposed a brittleness index considering the influence of water content and mechanical properties

1 Introduction

China is not only a big energy producer but also a major energy consumer, and China's natural gas demand is constantly increasing. Compared with 2001, China's natural gas consumption surged by 13.6 times to 372.6 billion cubic meters in 2021, with the degree of dependence on foreign natural gas reaching 44.29% (Liu, 2017). Consequently, ensuring a reliable supply of natural gas poses a significant challenge for China. Shale gas serves as a potential supply resource for conventional oil and gas resources. According to the statistics released by the United States Energy Information Administration (EIA), shale gas is mainly distributed in North America, Central Asia, and China, the Middle East and North Africa, and the Pacific Economic Cooperation Organization. The distribution of shale gas reserves across various regions worldwide is illustrated in Figure 1 (Liu, 2017). The total global shale gas reserves are about 206.6847 trillion cubic meters based on the statistics of EIA. The proven geological reserves in China amount to 31 trillion cubic meters and are the world's largest shale gas reserves. China's recoverable reserves of shale gas rank first globally, accounting for 15% of the world's total recoverable shale gas resources (Wang et al., 2013; Kim et al., 2015).

The continued improvements in geoscientific characterization are significant for reservoir evaluation and shale gas recovery (Montgomery et al., 2005). The hydraulic fracturing and evaluation of reservoirs sweet spots can be separated from the determination of various fundamental physical parameters (Wang W. et al., 2023; Deng et al., 2023). The composition and pore structure of shale plays crucial roles in determining the gas storage potential of shale gas reservoirs (Ross and Bustin, 2009; Yang et al., 2016a). However, the accurate measurement of shale pore structure remains challenging due to its complex and diverse nature. Previous studies have shown that the nanopore system as a critical factor controlling storage capacity of hydrocarbons and fluid flow in the fracture networks (Liu et al., 2024; 2017). The characterization methods of the pore structure of shale mainly include image analysis, fluid injection, and non-material injection (Maex et al., 2003). The non-material injection methods refer to nuclear magnetic resonance (NMR) (Su and Zou, 2016; Zhu et al., 2019), small-angle scattering, computerized X-ray tomography (CT), and thermal porosimetry method (Felix et al., 2012; Jannot et al., 2018). At present, scanning electron microscopy (Chen et al., 2011; Wang et al., 2012; Wei et al., 2013), mercury intrusion porosimetry, low-pressure nitrogen adsorption (Yang et al., 2013), NMR, etc., have been widely used in shale pore characterization (Chen S. et al., 2015; Hu et al., 2015; Yang et al., 2016b; Hu et al., 2016; Chen et al., 2017; Gao and Hu, 2018; Yuan et al., 2018). Shale pore size exhibits wide distribution; thus, it is usually difficult to comprehensively analyze all pore structures utilizing a single instrument or method. Therefore, several instruments and methods are often employed collaboratively to characterize and acquire shale pore structure information (Tian et al., 2012; Chen et al., 2015b). In a word, the microstructure and pore gap of the shale is mainly composed of parallel plates and ink bottle holes, characterized by amorphous pore features. The complexity of shale microstructure and pore gap poses a great challenge in understanding the evolution trend of gas adsorption and migration in pores and fractures.

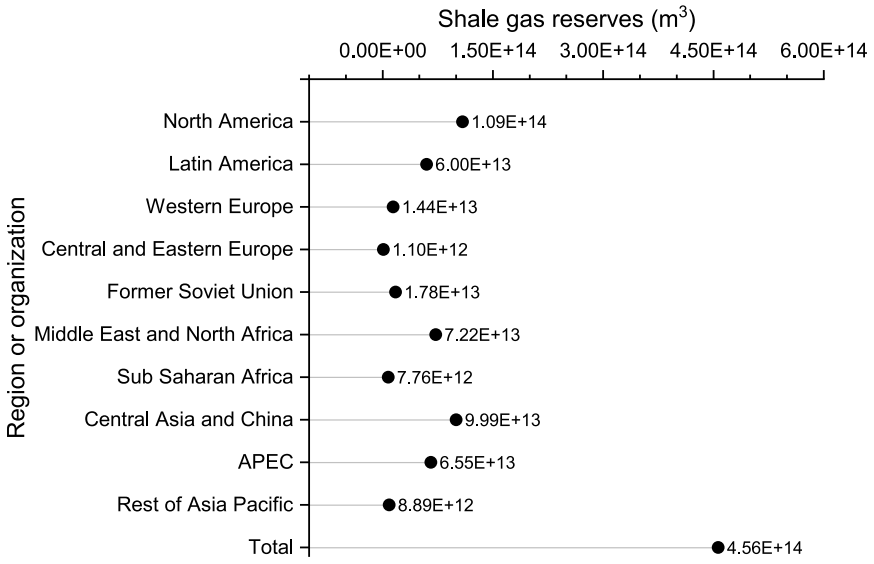

FIGURE 1
Shale gas reserves of different regions all over the world (Liu, 2017).

The shale brittleness index (BI) reflects the brittleness of shale and is an important parameter for evaluating the characteristics of shale reservoirs, which affects the development of shale gas. Generally, the shale with higher brittleness is easier to fracture and form fractures, which is beneficial to the extraction of shale gas (Li S. et al., 2022). The degree of rock brittleness failure can also be reflected by the significance of the peak strain. If the peak strain value is very low, the rock is more brittle. The porosity and pore structure, mineral composition, water content, etc. will directly affect the mechanical properties of shale and indirectly affect the brittleness index, and potential water-rock interaction further changes the mineral composition. The study delves into the correlation between these complex structures and mineral composition and investigates how mineral composition, as well as physical and mechanical properties (brittleness index, water content, mechanical strengths and parameters such as the cohesion, friction angle, Young's modulus of elasticity, Poisson's ratio), affect the evaluating of fracability, subsequent fracturing, and extraction operations in shale reservoirs. The correlation analysis of the brittleness index obtained by mechanical parameters and mineral components is conducted to explore the effect of shale mineral components and geostress. These are pivotal scientific and engineering issues worthy of attention. The study will investigate and discuss the influence of characterized parameters on the process and potential problems of shale fracability evaluation, fracturing, risk of injection-induced seismicity, wellbore stability, drainage, and operation management. Furthermore, corresponding suggestions on development and risk control will be put forward to address the engineering challenges associated with production and efficiency enhancement in gas shale reservoirs.

2 Specimen preparation and parameters characterizing

2.1 Shale specimen collection

The marine stratigraphic development area in southern China boasts favorable geological conditions for shale gas accumulation, harboring rich shale gas resources, which is an important strategic replacement field for China's oil and gas resources. The successful operation of China's first shale gas well (Wei-201) in Weiyuan, Sichuan in 2010, with a daily gas output of 2,000 m^3 from the Longmaxi Formation gas producing layer, marked the official commencement of China's shale gas development. Subsequently, the discovery and development of Fuling shale gas accelerated China's transition into the stage of commercial development. The specimens were collected from the outcrop profile of the Lower Silurian Longmaxi formation in Shuanghe town, Changning, Sichuan basin, as shown in Figure 2. This area is recognized as one of the favorable blocks for shale gas exploitation in China. The average thickness of shale is 100–500 m and the burial depth is 1500–4000 m. It is mainly composed of dark gray and black silty shale, carbonaceous shale, siliceous shale, and argillaceous siltstone. The original organic matter is mainly amorphous macerals, belonging to type I or II kerogen.

The microstructure and mineral composition of shale were primarily tested through powdered shale specimens. The preparation process of powdered shale used in this paper involves several steps, including crushing and screening of raw shale. About 200 mesh shale specimens were selected for the analyses and tests of X-ray diffraction (XRD), X-ray fluorescence (XRF), total organic carbon (TOC), vitrinite reflectance (*R*.o.), as shown in Figure 3, based on the results (Liu, 2017), and other analyses, small pieces (6 mm × 6 mm) were selected and used for electron microscope scanning, and about 60 mesh specimens were chosen for low-temperature N_2 adsorption analysis. Because the shale has distinct transversely isotropic bedding, measures to reduce core drilling disturbance were taken to reduce the influence of bedding on the brittle fracture characteristics of the specimens. Thus, the cores were drilled (Φ50 mm × 100 mm) along the vertical bedding direction, and specimens without macro structural plane were selected for the experiment.

Previous studies conducted by Dai et al. (2016) and Zhang et al. (2011) in this area have yielded pertinent data on the basic parameters of shale in this area. It was found that the range of the total organic carbon content of shale is 0.35%–18.4% (average value is 2.52%), the thermal maturity (using vitrinite reflectance to characterize) is 1.8%–3.6%, the range of the content of brittle minerals (quartz, calcite, dolomite, etc.) is between 47.6% and 74.1% and the average content of brittle minerals are 56.3% (Dai et al., 2016). In this study, the corresponding parameters were also measured. The relative tests revealed that the average *TOC* and *R*.o. contents of outcrop shale are 4.19% and 2.53%, respectively, which align with the ideal standards for shale gas reservoir evaluation ($TOC \geq 2\%$, $3\% \geq R.o. \geq 1\%$) (Zhang et al., 2011). In conclusion, the shale in the study area exhibits high thermal maturity.

2.2 Fundamental parameters characterizing

2.2.1 Low temperature N_2 adsorption

The low-temperature N_2 adsorption isotherm curve of shale was obtained by low-temperature N_2 adsorption test, and then the specific surface area and pore size distribution of shale were obtained. The specific surface area and aperture analysis were performed using an *Accelerated Surface Area and Porosity* (ASAP 2020m), i.e., automatic specific surface area and aperture analyzer with a specific surface analysis range of above 0.0005 $m^2 \cdot g^{-1}$ and pore size analysis range of 0.35 nm–300 nm. According to the classification standard of porous media of the IUPAC Association, shale pores are divided into three categories: macropores (>50 nm), mesopores (2–50 nm), and micropores (<2 nm). The specimen number of the BET test is S-238, with a specimen mass of 2.2483 g. Pretreatment was conducted to vacuum the shale specimen at 350°C for more than 10 h, and then the N_2 adsorption test was performed at liquid nitrogen temperature (−196°C). BET adsorption equation was used to calculate the specific surface area (S_{BET}), in which the total volume of specimen V_t (is the total pore volume of single point adsorption when $p/p_0 = 0.99$), mesopore volume (V_{mes}), micropore volume V_{mic}, mesopore surface area (S_{mes}), and micropore specific surface area (expressed by S_{mic})

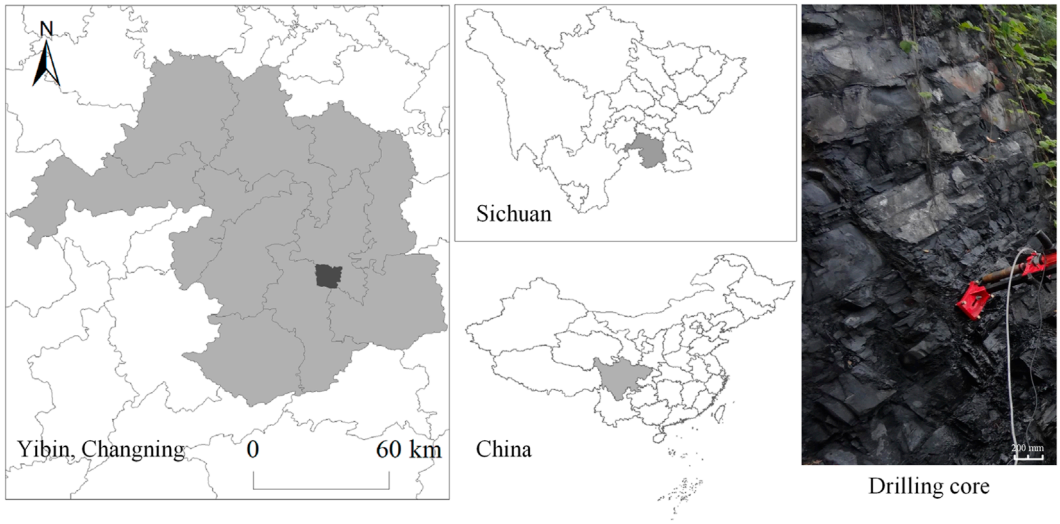

FIGURE 2
Sampling site at Changning in Sichuan, southwestern China.

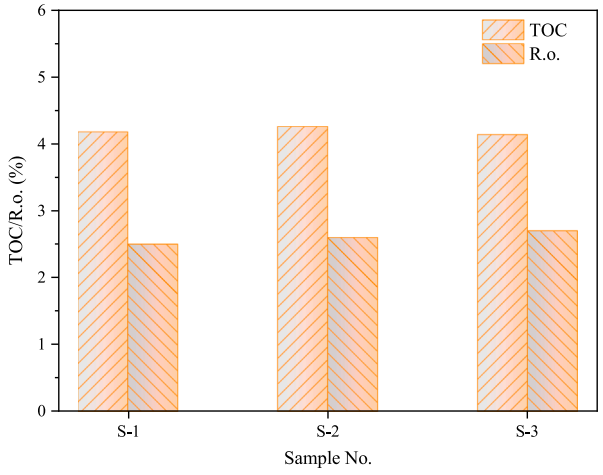

FIGURE 3
TOC & R.o. of shale sample from the outcrop profile of the Lower Silurian Longmaxi formation.

were calculated based on existing literature (Zhang et al., 2021; Zhang S. et al., 2023).

2.2.2 Analyses of scanning electron microscopy (SEM) and Raman spectrum

To characterize the microscopic pore and fracture structure of shale, the experimental specimens were scanned by electron microscope utilizing multiple magnifications to collect the pore shape of the shale. Before scanning, the observation surfaces of the experimental specimens were polished to achieve smoothness, and small square shale specimens measuring less than 10 mm × 10 mm were selected. The experimental equipment employed was the VEGAIILMU variable vacuum scanning electron microscope from the College of Materials Science and Engineering, Chongqing University. This equipment has "high-resolution" characteristics and a "fish eye" function, and is equipped with an XEDs energy spectrum probe. The minimum point resolution of the equipment is 3.0 nm, the maximum acceleration voltage is 30 kV, and the magnification is 4–100000 times.

The shale Raman spectrum was acquired using a laser confocal Raman spectrometer (HORIBA Jobin Yvon S.A.S, LabRAM HR Evolution) equipped with a × 100 objective lens of numerical aperture 0.9, at a working distance of 0.21 mm. An air cooled double-frequency Nd:Yag ($Y_3Al_5O_{12}$) green laser excitation avelengths (532 nm) with a −1 mm laser spot was adopted. The power of the laser for Raman measurements was maintained at 5 mW (50 mW with a 10% neutral density filter) to avoid sample heating and photoinduced damages. An integration time of 2 s was used in the measurements. The ND filter was set to 50% to prevent the sample from burning out and mitigate potential impacts on the measurement results.

2.2.3 Determination of element content and mineral composition

Mineral composition is an important factor affecting the physical and mechanical properties of shale. Therefore, it is necessary to test the mineral composition and element content. Shale oxide content can be used as the basic chemical characteristic parameter of shale to analyze the element content of shale. The mineral composition of shale was analyzed by XRD through which the XRD spectrum of shale core powder was obtained. The mineral composition was accessed using a German Bruker AXS D8 focus X-ray diffractometer under specific conditions: Cu target (monochrome), working voltage of 40 kV, working current of 30 mA, scanning speed of 3.85°/min, and slit width of 1 mm. Using standard powder diffraction data provided by the international data center of the powder diffraction Federation (JCPDS-ICDD), the material composition of the specimen was determined, and

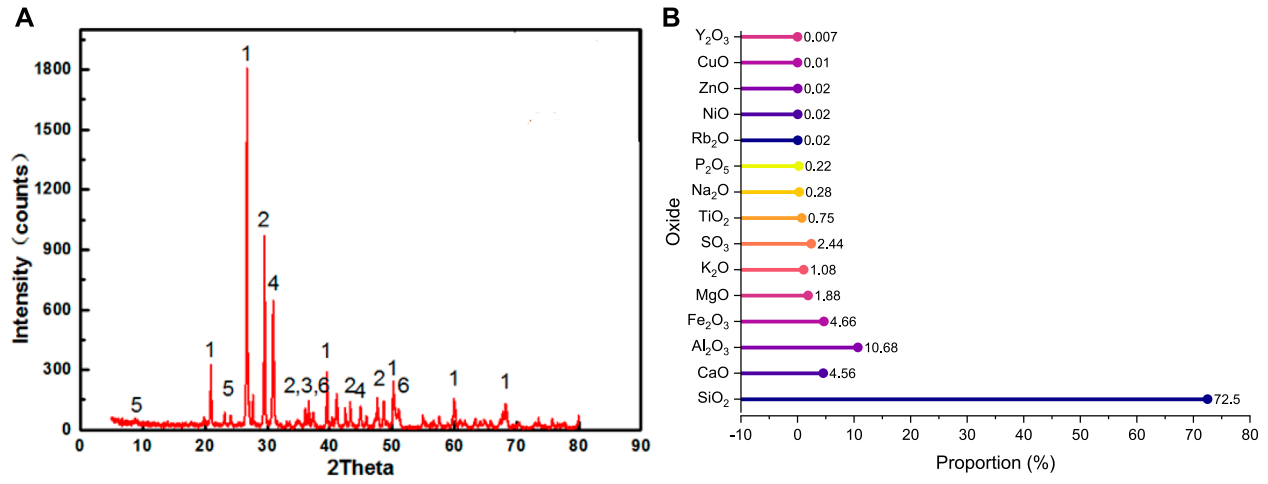

FIGURE 4
XRD spectrogram **(A)** and oxide content mass percentage of shale specimen **(B)** (Liu G.-J. et al., 2016; Liu, 2017).

the quantitative analysis was carried out according to the k-value method outlined in the international standard (GB5225). In addition, element content analysis was conducted using an X-ray fluorescence spectrometer to obtain various element contents of shale. After that, the element contents measured by XRF were converted into oxide contents.

At the micro level, the distribution of shale mineral components affects the micropore structure, which is related to the evaluation of gas content of shale gas reservoir. In particular, the clay minerals are conducive to shale gas adsorption; which can ultimately influence the design of shale artificial fracturing schemes and the evaluation of the fracturing effect at the macro level. The mineral composition of shale specimens was calculated by the adiabatic method, as illustrated in Figure 4 (Liu G. J. et al., 2016; Liu, 2017). The tested shale contains three brittle minerals: quartz, calcite, and dolomite. It can be concluded that the main minerals of shale are quartz and clay (illite and chlorite), and most of them also contain calcite, dolomite, pyrite, and other minerals. Clay minerals, significantly enhance shale gas adsorption and storage due to their large surface areas and pores. For example, the surface areas of illite and montmorillonite are 30 m^2/g and 800 m^2/g respectively (Kennedy et al., 2002; Xie et al., 2022). The high content of brittle minerals is conducive to artificial fracturing. In the case of Longmaxi formation shale in Changning, the content of brittle minerals (quartz, calcite, dolomite) is more than 50 wt%, indicating good fracability (Liu, 2017; Xie et al., 2022).

The element contents of shale measured by XRF are shown in Figure 4, with the elements converted into corresponding oxide forms. The shale mainly comprises Si, C, Ca, Al, Fe, K, Mg, and s, as well as some trace elements, such as Na, Rb, Ni, etc., all of which are less than 0.3 wt%. The content of the chemical composition of shale in nature varies within a certain range, and the SiO_2 content is generally between 45 wt% and 80 wt%. The SiO_2 content of shale specimens used in this study is 72.5 wt%, which is higher than that of general shale. Previous studies have demonstrated that the content of quartz determines the development degree of fractures (Li et al., 2019a).

3 Results and analysis

3.1 Microstructure analysis of gas shale

The microstructure of shale primarily comprises pores, fractures, and cracks, whose structures mainly include pore type, pore size, connectivity, porosity, pore-specific surface area, etc. The BET specific surface area (S_{BET}), pore volume, and pore volume of three types of pores calculated from low-temperature N_2 isothermal adsorption curve are shown in Table 1. The pore volume and specific surface area of the shale core are low, and there are three types of pores, namely, macropore, mesopore, and micropore. What's more, the proportion of mesopore specific surface area ($=S_{mes}/S_{BET}$) is 55%, the proportion of mesoporous pore volume ($=V_{mes}/V_t$%) is 79.5%, the proportion of micropore ranks second, while the proportion of macropore is the lowest, indicating that the quantity of mesopores exceeds that of micropores and macropores in these shale specimens. Numerous mesopores in shale are favorable for gas migration. This is consistent with the experimental results obtained in reference (Tang et al., 2011; Estrada and Bhamidimarri, 2016) for the Silurian Longmaxi formation shale in Pengshui, Chongqing. The low-pressure N_2 adsorption/desorption isotherm of the shale specimen at −196°C is shown in Figure 5 (left), and the pore size distribution of the shale specimen below 220 nm differential pore volume curve is displayed in Figure 5 (right).

The adsorption capacity of shale to N_2 increases with the growth of gas pressure within the range of 0.1–1.0 MPa (Figure 5). Notably, adsorption persists even in the high-pressure area, suggesting the existence of macropores. Besides, a hysteresis loop between the adsorption and desorption curves is observed. The formed hysteresis loop is caused by capillary condensation. The shape of the hysteresis ring reflects the micro shape of the pore structure. According to the shape classification of the hysteresis ring by IUPAC, the hysteresis ring shape of the shale specimen is H_2 type, in which the adsorption curve and desorption curve nearly coincide when the relative pressure is less than 0.4, indicating that shale holes contain numerous slit holes. Furthermore, according to the classification of

TABLE 1 Specific surface areas and pore volume of shale specimen (Liu, 2017) (The S_{BET} is the specific surface area obtained based on the BET method, S_{mic} is the micropore specific surface area, S_{mes} is the mesopore specific surface area, V_{mic} is the micropore pore volume, V_{mes} is the mesopore pore volume, V_{mac} is the macropore pore volume, and V_t is the total pore volume).

Shale specimen	$S_{BET}/m^2 \cdot g^{-1}$	$S_{mic}/m^2 \cdot g^{-1}$	$S_{mes}/m^2 \cdot g$-1	$V_t/cm^3 \cdot g^{-1}$	$V_{mic}/cm^3 \cdot g^{-1}$
	21.7305	7.1827	11.826	0.0207	0.0032
S-238	$V_{mes}/cm^3 \cdot g^{-1}$	$V_{mac}/cm^3 \cdot g^{-1}$	V_{mic}/V_t/%	V_{mes}/V_t/%	V_{mac}/V_t/%
	0.01645	0.00105	15.5	79.5	5

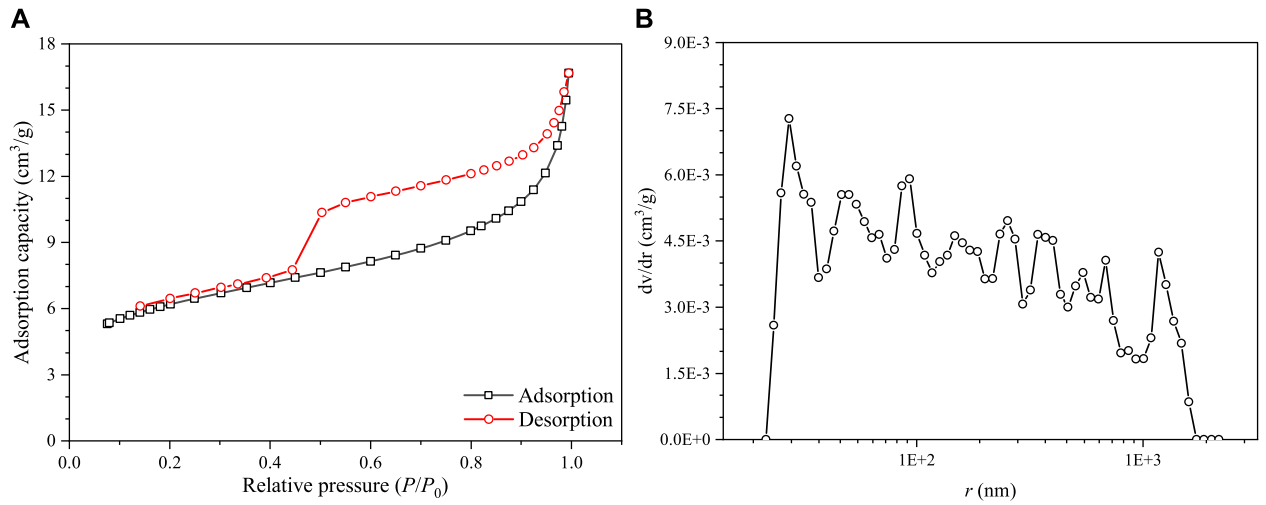

FIGURE 5
Low pressure N_2 isothermal curves at temperature −196°C **(A)** and pore size distribution **(B)** (Liu, 2017).

isotherms by IUPAC, the adsorption curve measured at −196°C low-temperature N_2 belongs to a type II isotherm, indicating monolayer adsorption.

Figure 6 presents the SEM diagram of shale pores under four different magnifications. From the SEM images of different multiples, the mineral particles inside the shale are closely arranged, the average pore size is small, and the connectivity is poor, indicating that the reservoir is highly compact. In addition, the shale exhibits a wide range of pore types and special pore and fracture structures. Furthermore, it can be seen from Figure 6 that the shale pore structure is complex and diverse, and the geometry of shale mineral particles is very different. Besides, there are many grains on the shale surface, and many debris particles float on the shale surface and pores. The grains on the shale surface in the figure are mainly composed of clay minerals and silicates. Their shape changes due to compaction during diagenesis and the softer clay minerals are gradually compacted. Finally, the harder minerals and clay minerals form intergranular pores (Ning et al., 2017). These shale fragments, comprised of inorganic minerals, fill extensive fractures and cracks, and increase the intergranular porosity of shale.

Drawing upon the research basis on the micropore structure of shale reservoirs (Ji et al., 2012), in conjunction with the observations from Figure 5 and Figure 6, it becomes evident that the pores in shale mainly include intergranular pores, dissolution pores on the surface of mineral particles, internal pores of organic matter and microfractures, which serve as important storage spaces and seepage channels for shale gas. These pores are unevenly distributed on the shale surface, and there is stratification between large particles. The development of micropores suggests that there is a large storage space in shale. Microfractures and macropores function as flow channels for shale gas, and a good pore fracture network is a necessary condition for shale gas exploitation. The microscopic heterogeneity and mechanical anisotropy characteristics of shale not only influence the spatial anisotropy of its physical and mechanical parameters but also affect the propagation behavior of hydraulic fractures during fracturing to a large extent.

Raman Spectroscopy is treated as the indication of thermal maturity probe in shale petroleum systems (Hackley and Lünsdorf, 2018). The characteristic Raman spectrum of carbonaceous materials generally has two stages, which mainly include two spectral bands, namely the D1 peak band (−1350 cm^{-1}) and the G peak band (−1580 cm^{-1}), reflecting the order degree of carbonaceous materials. The position of the Raman peak changes with the variation of particle and pore size. The smaller particle size will shift the peak position, widen the peak asymmetry, and weaken the peak intensity. In the study, the D1 peak band is at 1324.9 cm^{-1}, and the G peak band at 1596.9 cm^{-1}. The I(D)/I(G) refers to the intensity ratio of the D-peak to the G-peak, and a higher ratio indicates that the C atom crystal has more defects. In the study,

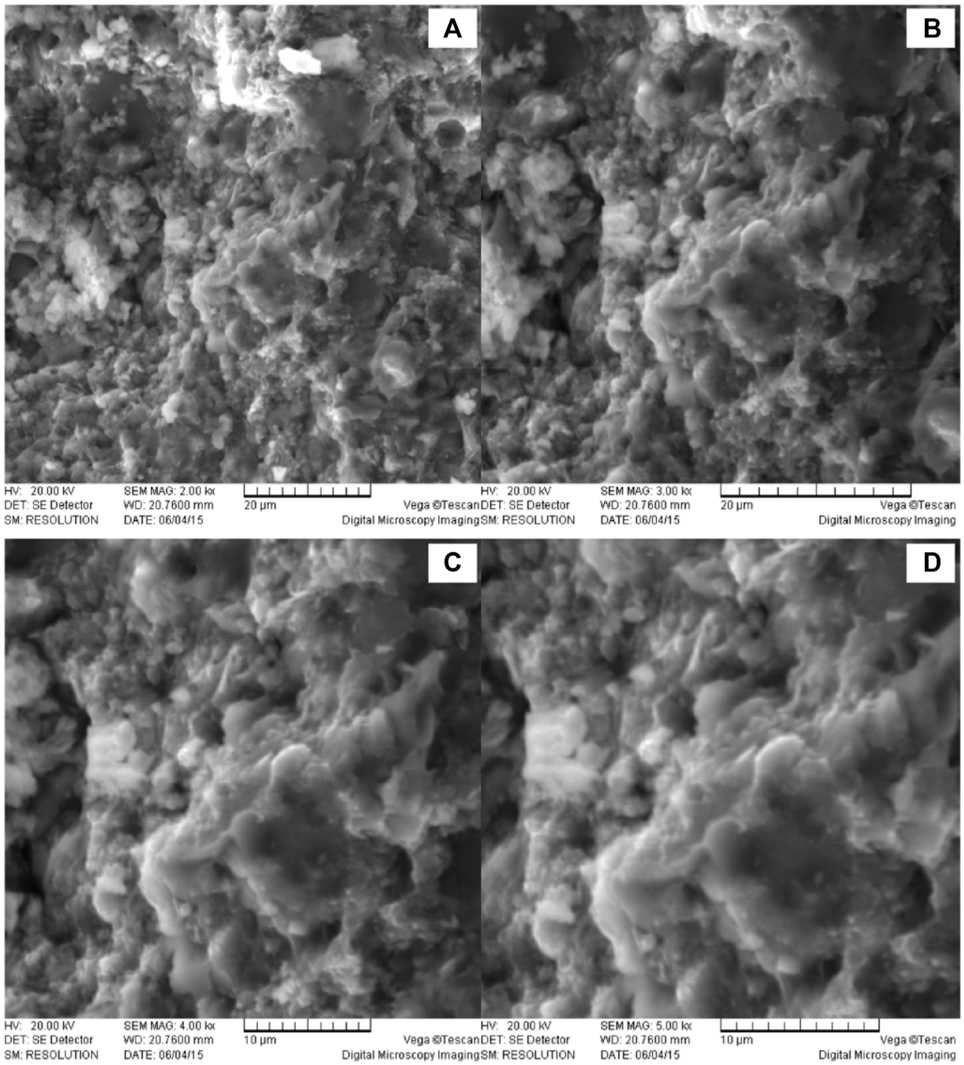

FIGURE 6
Microstructure of shale based on scanning electron microscope images: **(A)** 2 kx; **(B)** 3 kx; **(C)** 4 kx; **(D)** 5 kx (Liu, 2017).

the ratio of I(D)/I(G) is 0.77 while the corresponding integral areas values ratio of D and G peaks is 2.40, as shown in Figure 7.

Nuclear magnetic resonance T_2 spectroscopy stands as a reliable method to quantitatively characterize the microscopic pore structure of reservoirs (Bai et al., 2016; Fan et al., 2023; Zhang et al., 2023). The relationship between shale pore size distribution and pore radius obtained by the NMR test is shown in Figure 8 (Liu, 2017; Liu et al., 2017), and the pore size distribution and pore throat distribution are shown in Figure 9 (Liu, 2017; Liu et al., 2017). Additionally, the initial NMR characteristic parameters of shale specimens are displayed in Table 2 (Liu, 2017). The pore size of the shale core measured by NMR is predominantly distributed within the range of 5–237 nm, mainly in medium and large pores, as illustrated in Figure 9. These experimental findings are consistent with those of Zou Cai et al., in 2010 (Zou et al., 2010; Zou et al., 2011). As observed, the distribution of pore throats within 250 nm accounts for 7.7%, while that of larger pore throats with more than 250 nm takes up about 92.3%. Table 2 outlines the initial NMR characteristics of shale specimens. The permeability of the shale core is 4×10^{-4}–2×10^{-3} mD and porosity is 3.55–4.2%, demonstrating that the permeability and porosity of the original rock core are very low.

Based on the above results of low-temperature N_2 adsorption, mercury injection test, nuclear magnetic resonance test, and SEM analysis, the pore structures and sizes measured by the four common characterization methods show certain differences. Shale pore sizes measured via the low-temperature N_2 adsorption method mainly fall within the range of 2–220 nm, while those measured by mercury porosimeter and NMR are mainly distributed in 200 nm–0.18 mm and 5–237 nm respectively. Upon integrating the pore size distributions obtained from these three test methods, it is evident that the measured shale pore size distribution range spans from 2 nm to 0.18 mm, illustrating a wide shale pore size range. SEM analysis mainly reflects some minerals and pore characteristics of shale from the surface, but cannot quantitatively analyze the pores like the three aforementioned methods. The results from the three

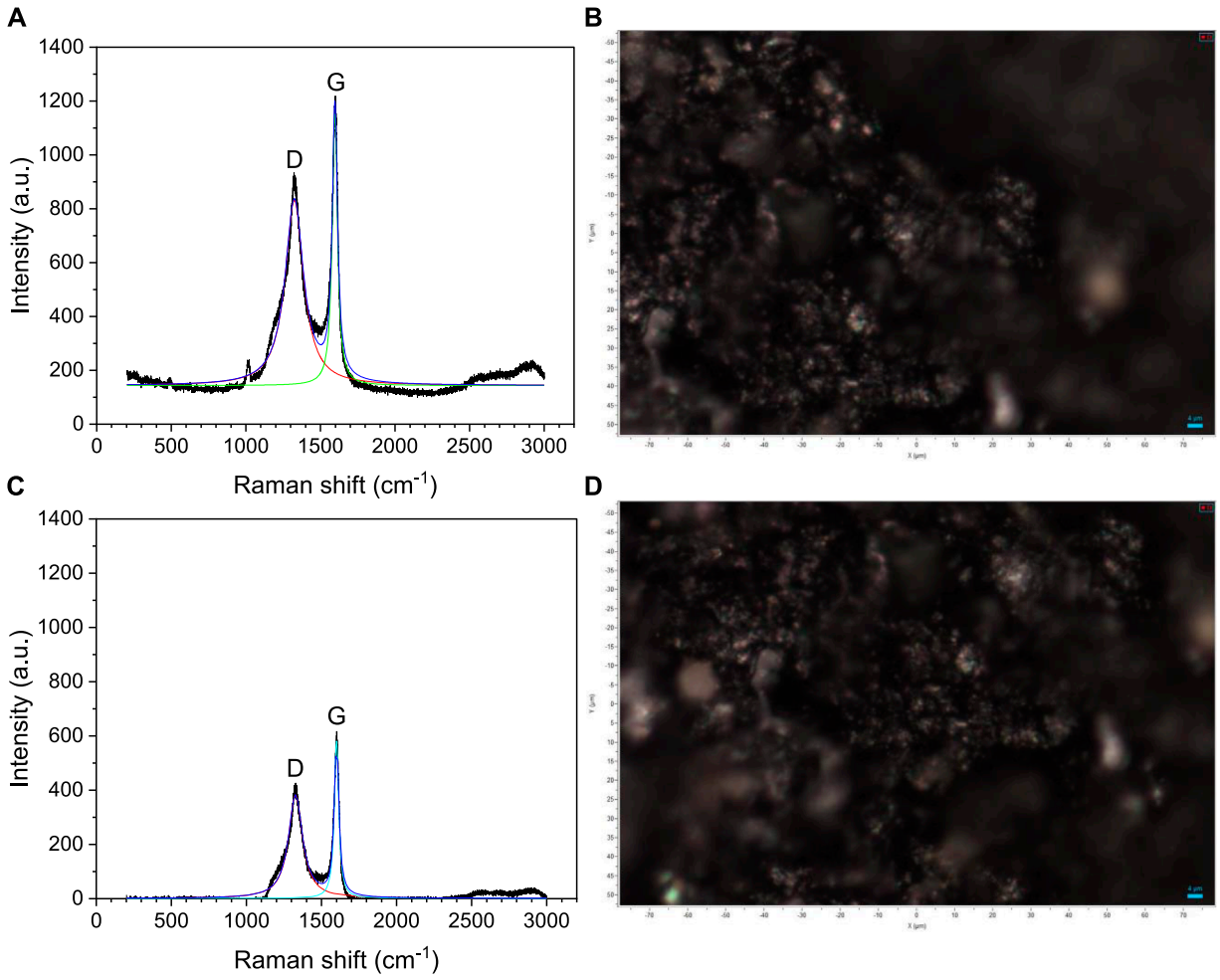

FIGURE 7
Raman spectrum of shale sample. (Laser: 532 nm; acq time: 2 s; accumulation: 2 s; objective: ×50 LWD; ND filter: 50% **(A)** & **(B)**/25% **(C)** & **(D)**).

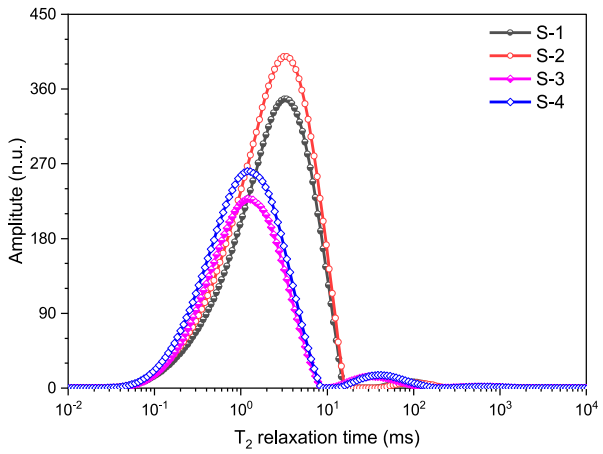

FIGURE 8
NMR T_2 relaxation spectra of shale specimens (Liu, 2017; Liu et al., 2017).

tests which have their unique characteristics indicate the presence of nano-pores in shale. The pore size scale of the NMR test is consistent with that of the low-temperature N_2 adsorption test, which is mainly used to characterize the different degrees of test pieces and matrix permeability characteristics. Given the broad distribution of shale pore size, it is difficult to completely measure and reflect the pore structure of shale by a single test method. Therefore, this study uses four test methods to characterize the pore structure of shale, enabling a comprehensive and systematical characterization of the micropore and fracture of shale.

3.2 Determination of total organic carbon and vitrinite reflectivity

The abundance of organic matter profoundly impacts the development degree of organic matter pores in shale. The total organic carbon contents of the shale specimens are as follows: 4.18% (T-1), 4.26% (T-2), 4.14% (T-3), with an average of 4.19%. Those

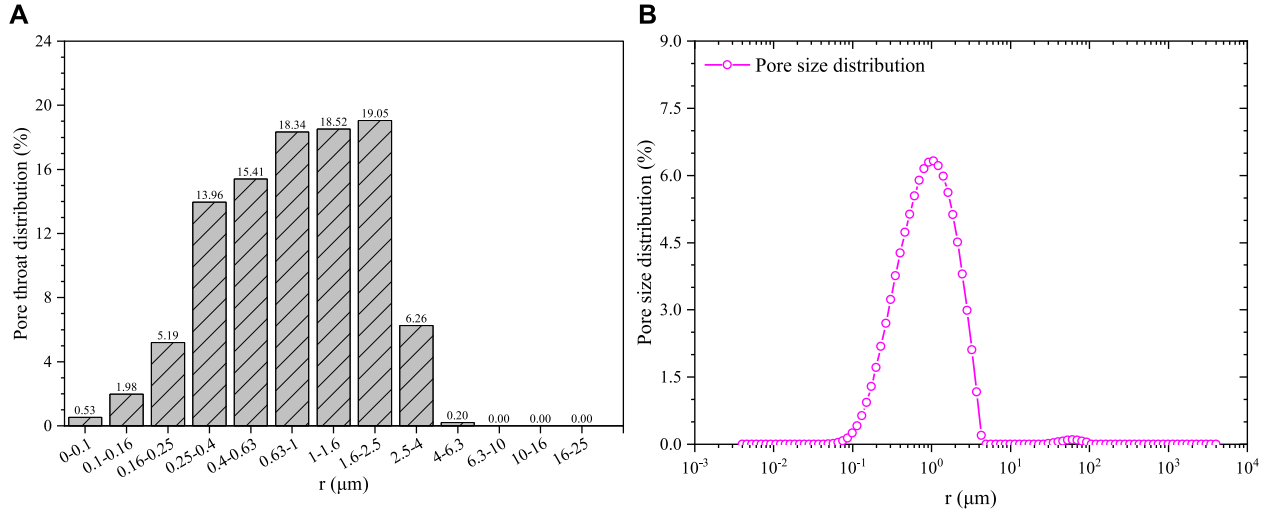

FIGURE 9
Pore throat distribution of shale specimens **(A)** and pore size (pore diameter *r*) distribution **(B)** (Liu, 2017; Liu et al., 2017).

TABLE 2 NMR parameters of shale specimens.

Specimen number	S-01	S-02	S-03	S-04
The total area of initial T_2 spectrum	8290.3	8365.2	8245.4	8653.5
Initial NMR porosity/%	3.56	3.66	3.79	4.20
permeability/10^{-3} mD	0.4	0.9	1.4	2.0

values indicate a notably high *TOC* content of the shale specimens taken from Changning area, ranging between 4.14% and 4.26%. In evaluating shale gas reservoirs, the total organic carbon content serves as a main index to characterize the organic-rich shale, while the brittleness index is crucial for evaluating fracturing quality. Therefore, integrating organic carbon content and brittleness index enables a more nuanced depiction of the "dessert layer" distribution, providing a favorable basis for exploration and development. Based on the significant correlation between the brittleness index and *TOC*, Zhang et al. established a classification standard of shale gas reservoir quality by integrating the organic matter abundance and fracturing ability of shale. According to this standard, high-quality reservoirs (desserts) are those with *TOC* > 3% and BI > 50%, sub-optimal reservoirs with 2% < *TOC* < 3% and 40% < BI < 50%, poor reservoirs with 1% < *TOC* < 2% and 30% < BI < 40% and non-reservoirs with *TOC* < 1% and BI < 30% (Zhang et al., 2016; Wang et al., 2020). Liu et al. proposed a *TOC* correction method to address the influence of *TOC* content on brittleness index evaluation (Liu et al., 2015), which has been applied in multiple wells and achieved positive results. Based on the measured *TOC* content of shale specimens and the brittleness index range, in accordance with the above reservoir classification standards, it can be concluded that Changning area, from which the selected shale specimens were taken, is a favorable area for shale gas development and exploitation (Hou et al., 2019; Cheng et al., 2022).

The thermal maturity test results for the shale specimens are as follows: 2.4% (sample R-1), 2.5% (sample R-2), 2.7% (sample R-3), with an average of 2.53%. Vitrinite reflectance (*R.o.*) is the most widely used, effective, and important index for evaluating organic matter maturity and thermal evolution in the world. It can reflect the maturity level of organic matter in most source rocks since the late Paleozoic to a certain extent.

4 Brittleness index considering mechanical properties and minerals composition

4.1 Brittleness index of shale based on mechanical properties

There are various ways to evaluate the brittleness of shale based on mechanical properties such as sonic velocities, elastic properties, and mineral composition, etc (Li Y. et al., 2022). Shale brittleness index is affected by many factors, including the mineral composition of shale, rock structure, diagenesis, etc. For example, the higher the content of brittle minerals such as quartz, the higher the brittleness index of the shale, conversely, while the higher the content of plastic minerals such as clay, the lower the brittleness index of the shale. When using mechanical parameters to quantify the brittleness index, the shape and pattern of the post-peak stress-strain curve obtained from laboratory experiments has been a primary method to quantitatively understand the degree of rock brittleness. If the strength of the rock drops rapidly to a specific low value after reaching its peak, it indicates a high degree of brittleness. Conversely, if the post-peak strength decreases slowly or even does not decrease, the degree of brittleness is very low. Based on this, this study evaluated brittle characteristics of rocks under both simple stress states (uniaxial) and triaxial stress states (with confining stress) by

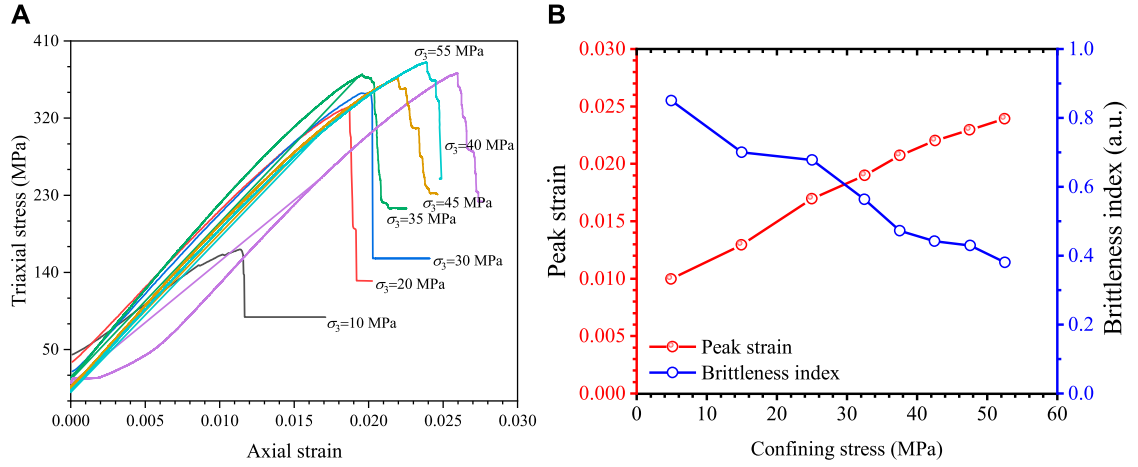

FIGURE 10
Conventional triaxial tests under different confining stresses σ3: **(A)** triaxial stress-strain curve; **(B)** peak strain-confining stress curve (Liu G. J. et al., 2016; Liu, 2017).

quantitatively investigating relative magnitude and absolute rate of post-peak stress reduction according to Formula 1 (Bishop A, 1967).

$$B_1 = \frac{\sigma_p - \sigma_{res}}{\sigma_p} \tag{1}$$

In the formula, B_1 represents the post-peak brittleness index of the rock, with values ranging from 0 to 1, where a higher value indicates greater brittleness. σ_p is the peak intensity; σ_{res} is the residual strength. The evolution of mechanical parameters obtained by conventional triaxial compression experiments under different horizontal confining stress conditions is depicted in Figure 10 and Table 3, according to the results of Liu G. J. et al. (2016). It is obtained from the brittleness evaluation based on mechanical tests that the maximum and minimum peak strain parameters of shale in Changning area are 2.40% and 0.96%, respectively. What's more, with the increase of confining stress, the brittleness of shale gradually decreases, while the corresponding peak axial strain at failure rises sequentially. Hucka and Das (1979) found that a low elongation value signifies higher brittleness of the rock (Hucka and Das, 1974). This implies that the lower the strain at failure, the greater the degree of brittleness. Additionally, the method of evaluating brittleness relative to mineral components can directly reflect the mechanical properties of shale under different stress states and in different layers, and can better evaluate the difference in brittleness of shale specimens.

4.2 Shale brittleness index based on mineral composition

Brittle minerals mainly refer to quartz, feldspar, calcite, dolomite, and pyrite. Quartz and feldspar are the basic and most important rock-forming mineral components making up rock formations in the earth's crust and very few of these minerals deposited from externally migrated debris. Pyrite is a secondary mineral rich in organic matter and newly formed in a reducing environment. Carbonate minerals, such as calcite and dolomite, are mostly formed by chemical deposition. They have brittle mechanical characteristics and are usually classified as brittle minerals (Nelson, 2001; Jarvie et al., 2007; Matthews et al., 2007; Rickman et al., 2008; Wang and Gale, 2009; Diao, 2013; Li, 2013; Jin et al., 2014). For North American shale, quartz is typically used as a molecule to calculate the brittleness index. However, due to the complex reservoir conditions in southern China, where shale compositions often include brittle minerals such as quartz, calcite, and dolomite, this study calculated the brittleness index based on the results of Liu et al. (2016). The calculation formula is shown in Eq. 2.

$$B_2 = \frac{C_{quartz}}{C_{quartz} + C_{calcite} + C_{clay}}$$
$$B_3 = \frac{C_{quartz} + C_{calcite} + C_{dolomite}}{C_{quartz} + C_{calcite} + C_{dolomite} + C_{clay}} \tag{2}$$

Here C_{quartz}, $C_{calcite}$, $C_{dolomite}$, and C_{clay} represent the contents of different minerals (quartz, calcite, dolomite, and clay) of the shale sample, respectively. North American shale generally uses B_2 in Formula 2 to calculate the brittleness index; in view of the relatively complex mineral composition of Paleozoic shale in southern China, this study uses the brittleness index B_3 to evaluate the brittleness of shale. For shale with complex mineral composition, the brittleness index should be calculated according to B_3 in Formula 2. If the feldspar content is significant, the feldspar should also be accounted for in brittle minerals content of the Formula 2.

However, shale reservoirs situated in deep formations are usually subject to three-way anisotropic compressive stress conditions, and there are effects of pore fluids such as reservoir water, hydraulic fluids, oil, and gas. Therefore, the brittleness index should also be improved accordingly to adapt to the optimization of technical parameters for shale development in deep formations. Previous studies have shown that moisture content directly affects the physical and mechanical parameters of shale (Zhang et al., 2006). The relationship between mechanical parameters and moisture content can be abstracted, where Young's modulus of elasticity $E = a_0 w^{b_0}$, cohesion $c = c_0 e^{a_1 \omega + b_1}$, friction angle $\varphi = \varphi_0 e^{a_2 \omega + b_2}$, Poisson's ratio $v = a_3 w + b_3$, and the other symbols represent constant correlation

TABLE 3 Calculating results of brittleness index for shale specimens (Liu et al., 2016; Liu, 2017) (σ_3 is confining stress; E is Young's elastic modulus; ν is Poisson ratio; σ_p is peak strength; ε_3 is peak strain; B_1 is post-peak brittleness index. According to Dinik formula (Xie, 2007): $\sigma_2 = \sigma_3 = \sigma_1\nu/(1\text{-}\nu)$, shale Poisson ratio ν is 0. 20–0. 40, the natural bulk density of shale is 23.0–26.2 kN/m^3. In the article, ν =0.25 and γ =23 kN/m^3 are selected, then the experimental design stress states should satisfy $\sigma_2 = \sigma_3 \geq 7.6H$, σ_i (i =1, 2, 3) $\geq 12.7H$, where σ_i (i =1, 2, 3) is the average *in-situ* stress; H is burial depth of the shale reservoir).

Sample No.	σ_3 (MPa)	E (GPa)	ν	σ_p (MPa)	ε_p (%)	σ_{res} (MPa)	ε_{res} (%)	B_1
S-1	0	12.35	0.32	125.8	0.96	0	1.1	≈1
S-2	10	12.54	0.38	126.8	1.033	37.76	1.35	0.70
S-3	20	15.6	0.26	282	1.56	80.25	1.68	0.71
S-4	30	17.3	0.34	300	1.85	106.25	2.06	0.646
S-5	35	20	0.25	310.66	1.95	166.09	2.13	0.482
S-6	40	17.65	0.42	322.29	2.19	172.74	2.34	0.464
S-7	45	18.82	0.299	327.82	2.20	189.8	2.51	0.42
S-8	50	19	0.23	334.656	2.38	187.96	2.48	0.438
S-9	55	18.9	0.297	326.87	2.40	221.204	2.68	0.323

coefficients; Here the a_i, b_i, c_i (i = 0, 1, 2, 3) is the fitting constants. To this end, a brittleness index that accounts for the state of water and the combined influence of stiff minerals and clay minerals is proposed, as depicted in Eq. 3.

$$B_{sh} = \frac{C_{quartz}}{1 + wC_{clay}} + \frac{(C_{calcite} + C_{dolomite})(1 - w)}{C_{quartz} + C_{calcite} + C_{dolomite} + C_{clay}} \tag{3}$$

The w in Eq. 3 is the water content of the shale rock, which can be calculated according to Eq. 4, derived from the basic physical and mechanical parameters of shale.

$$w = \begin{cases} \ln\left(\frac{c}{c_0}\right)^{-a_1} - \frac{b_1}{a_1} \text{ or } \ln\left(\frac{\varphi}{\varphi_0}\right)^{-a_1} - \frac{b_2}{a_2} \\ \frac{E}{a_0} - \ln b_0 \text{ or } \frac{\nu - b_3}{a_3} \end{cases} \tag{4}$$

In this study, a brittleness index considering the influence of water state and the mechanical parameter is proposed, i.e., brittleness index B_{sh}, as shown in Eq. 3. In addition, the influence of the composition of various minerals in this brittleness index can more truly reflect the brittleness index of deep formation. The results of the study are consistent with the results of this study by Chen and Xiao (2013), the evaluation of shale brittleness and the analysis of mineral composition in shale samples revealed that the shales in southern Lower Cambrian, Upper Ordovician-Lower Silurian and Upper Permian exhibited higher average brittleness index, and the three sets of shales samples displayed higher levels of brittleness (Chen and Xiao, 2013). Therefore, these shale formations exhibit good fracability, providing compelling evidence for shale gas development in this region.

The brittleness index of shale correlates positively with quartz mineral content but inversely with clay mineral content. From the results of mineral component tests, the most developed and highest content clay mineral in the study area is illite. The content of chlorite ranks second only to illite, while the presence of kaolinite, Eamonn mixed layer and montonite is comparatively lower, though they still constitute significant components. Among the mineral content of the outcrop samples from the Longmaxi Formation, the content of brittle minerals is nearly 58.7%. The control exerted by mineral components on brittleness is evident from the fact that altering the mineral composition can change its brittleness. In general, an increase in the content of brittle minerals such as quartz, feldspar, and calcite, enhances the fracability of the formation. The brittleness index of the mineral components for each shale specimen was calculated using Eqs 1–4, as illustrated in Figure 11.

5 Discussion and future research

5.1 Effect of shale mineral components on physical and mechanical parameters

Mineral components have an important influence on both the composition of pore fractures and the stability of wellbore. Clay minerals and brittle mineral components such as quartz, calcite, dolomite, and feldspar (the feldspar content in shale is usually minimal) exert significant influence on the mechanical properties of shale. Brittle minerals typically have higher hardness and brittleness. When shale is subjected to external loads, stress concentration easily occurs between these mineral particles, leading to brittle fracture failure; and the mechanical strength is relatively great, and the corresponding peak strain is relatively low. Conversely, if the content of clay minerals increases in shale, its strength and brittleness can decrease accordingly, and the pre-failure plastic deformation will increase accordingly. Shales with high brittle mineral content are rich in microfractures in diagenesis, while shales with high clay mineral content tend to exhibit lower mechanical strength and brittleness, smaller average pore size, reduced pore connectivity, and denser reservoirs. Due to the influence of pressure solution effects and water-rock chemical interactions, as well as later fracturing

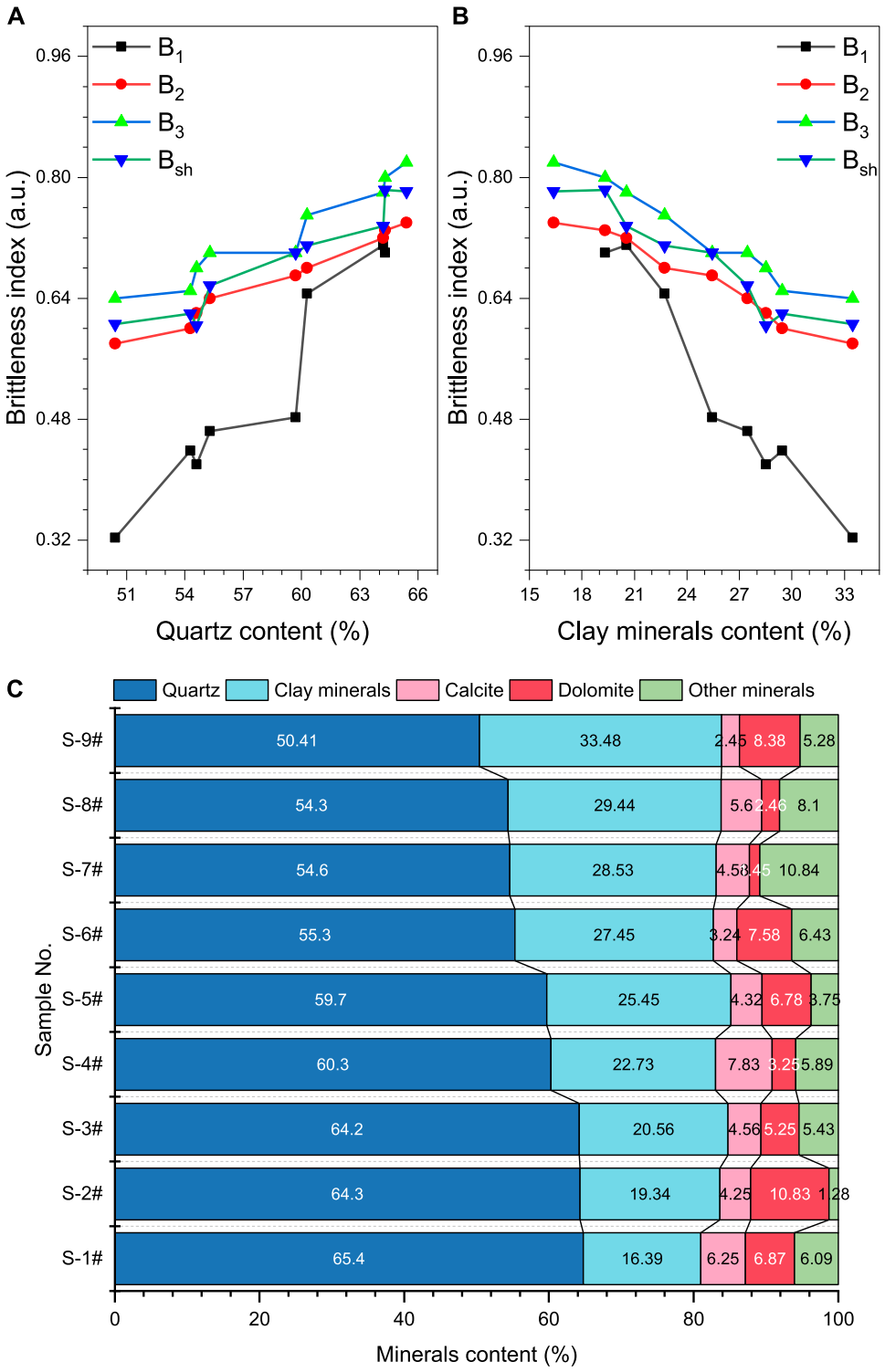

FIGURE 11
Relationship between brittleness index and content of quartz **(A)** and clay minerals **(B)**, and minerals components of shale samples **(C)** (Liu et al., 2016; Liu, 2017).

fluid, the pores of such shale are susceptible to alteration through the dissolution-sedimentation process of minerals. Consequently, some pores may become filled and blocked, losing connectivity. Future research should pay close attention to the combined effects of mechanical and chemical factors on wellbore stability, develop corresponding reinforce measurements both in technique and materials such as shale inhibitors (Wei et al., 2021), and utilize prediction methods and models employing the newly developed

approaches in big data and artificial intelligence (Barham et al., 2021).

Based on the above low-temperature N_2 adsorption, NMR test and SEM analysis results, the two commonly used pore structure characterization methods yield different ranges of pore size measurements. The shale pore sizes measured by the low-temperature N_2 adsorption method predominantly fall within the range of 2–220 nm, while those measured by NMR are primarily distributed between 5 and 237 nm. By integrating the pore size distribution results from these two test methods, the measured shale pore size distribution range is 2 nm–0.18 mm, indicating a wide shale pore size range. SEM primarily reveals certain minerals and pore characteristics of shale from the appearance, but it can't quantitatively analyze pores like the first two pore measurement methods. Results from N_2 adsorption and NMR tests indicate the presence of nano pores in shale. The pore size scale observed in the NMR test aligns closely with that of the low-temperature N_2 adsorption test, which is mainly used to characterize the degree of difference of specimens and the permeability characteristics of the matrix. Due to the wide distribution range of shale pore size, it is difficult to completely measure and reflect the pore structure by a single method. Therefore, this study employs three methods to reflect the micro pore and fracture characteristics of shale comprehensively and systematically. In a study conducted by Li Wenbiao et al. (Li et al., 2019b), a substantial proportion of 30 specimens from the southern marine Wufeng and Longmaxi formation were analyzed using low-temperature nitrogen adsorption method and three types of shale were identified according to the hysteresis loop curve such as Figure 5A. The results show that: clay mineral mainly develops tabular pores, with larger apertures ranging from micropores (<2 nm) to macropores (>50 nm) being relatively developed; organic matter mainly develops ink-bottle-shaped pores, mainly with the sizes of micropores and mesopores (2–50 nm). These findings are consistent with conclusions of this study.

Different rock mineral compositions and geological structures have a great impact on shale gas development. Results from conventional physical and mechanical tests may diverge significantly from actual reservoir environmental conditions that enrich in geological fluids and temperature-stress coupling in deep formations, thus it is necessary to extrapolate and correct the obtained mechanical parameters. In essence, the scientific characterization and determination of petrophysical and mechanical parameters are fundamental and crucial for shale gas development. In addition to mechanical strengths, Young's elastic modulus, and other mechanical parameters, lithology and rock mineral composition are the main internal factors controlling the development of fractures. The adsorption capacity of shale gas is related to mineral composition, organic matter content, specific surface area, temperature, geostress and pore pressure of shale. As shown in Figure 12, shale with high quartz content tends to exhibit greater brittleness, which facilitates the formation of natural cracks and induced cracks under external forces, making it conducive to shale gas extraction. In hydraulic fracturing operations, preference should be given to brittle shales with high Young's modulus, low Poisson's ratio, and a rich organic matter content. Poisson's ratio and Young's modulus serve as indicators of rocks' deformation properties, especially in the aperture maintenance of fractures after rock fracture. A lower Poisson's ratio indicates higher brittleness of the rock, while an increase in Young's modulus correlates with enhanced brittleness in the rock. Therefore, shale reservoirs at different depths should account for corresponding technical parameters of fracturing stimulation and extraction in reservoir fracturing and mining based on their specific mineral compositions.

However, the difference between the two brittleness evaluation methods employed to analyze samples may stem from the mineral composition method's sole focus on mineral composition while disregarding other influential factors such as diagenesis, tectonic action, abnormal pressure, etc. Diagenesis is the most important one among those factors. Shale brittleness is a kind of comprehensive characterization, resulting from the combined influence of mineral components, cementation (material) type, structure, and other factors. The important role of brittleness is not only reflected in the effect of shale fracturing, but also in the development of pore fractures during and after the diagenetic process. In this study, samples from the lower shale of the Longmaxi formation, which has a high organic carbon content and is considered an important potential layer, were selected. Notably, the upper part of the Longmaxi formation contains more sand while the lower section contains less. Therefore, attention should be paid to the sampling position during the evaluation. The longitudinal composition change of Longmaxi formation will cause the longitudinal change of its fracturing effect. It is essential to note that the brittleness index of the upper layer alone cannot adequately represent the brittleness index of the lower layer or the entire Longmaxi formation. A comprehensive brittleness evaluation considering different mineral components and contents is necessary to reflect the brittleness characteristics of this group of Longmaxi formation. It is crucial to recognize that the brittleness of shale is influenced by both mineral composition and stress state. Therefore, when selecting fracturing levels and layers, as well as accessing fracability, it is imperative to carefully consider the on-site stress state and shale mineral composition.

5.2 Shale gas production, carbon dioxide storage, and disaster risk

The basic physical and mechanical parameters of shale will affect the fracturing and permeability enhancement and the gas/liquid seepage characteristics of the reservoirs after the stimulation such as by the hydraulic fracturing (Zhou et al., 2016; Liu G. et al., 2017; Liu G.-J. et al., 2017). The evolution of shale petrophysical structure can affect the gas storage through multiple factors and multiple stages of tectonic constraint effect (Gao et al., 2023; Zhao et al., 2023). The impact of nanopores on gas flow is complex; in shale gas production, understanding their influence on gas flow is crucial for optimizing production strategies and enhancing output. Nanopores in shale possess a significant specific surface area and capable of adsorbing gas, thereby affecting gas adsorption/desorption processes, and thus affecting gas migration within the shale strata. It can be seen from the shale outcrop at the sampling site that, the natural fractures of shale reservoirs in this area are highly developed due to the influence of multi-stage geological structure processes (the process of crustal movement or rock formations under the

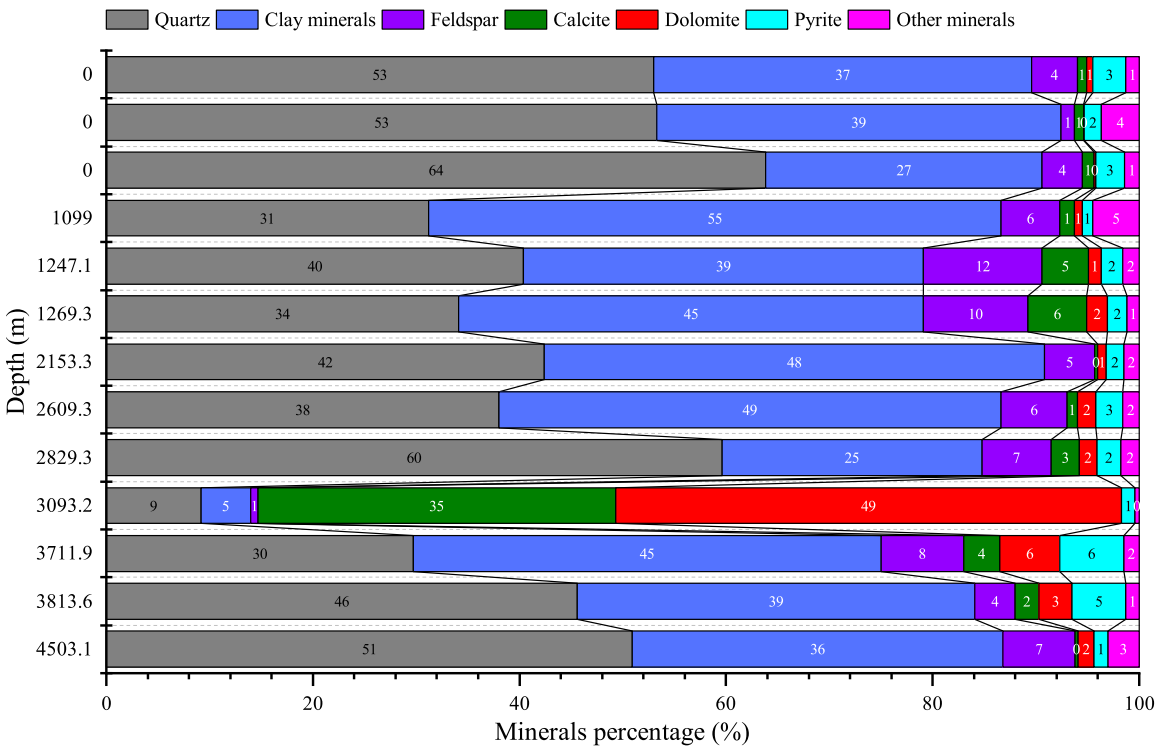

FIGURE 12
Mineral percentage change with the burial depths of Longmaxi shale samples (Yang et al., 2021).

action of the earth's internal forces), the thickness and reserves are quite considerable, and the brittle minerals are moderate, which is conducive to enhancing the area as an energy base for large-scale commercial development, indeed, the shale gas reserves and development potential in this region are notably vast. After fracturing transformation, the reservoir pressure is expected to drop below the desorption pressure, promoting the release of gas from the microporous surface of shale. Subsequently, the gas diffuses into the fracture system of the shale, and then seeps through the fracture system to the fractures and finally accumulates within them before flowing to the wellbore. This process is illustrated in Figure 13. In the near-wellbore section, due to fracturing stimulation and drilling relief, the shale reservoir is damaged and generates cracks and fractures. During the crack seepage process, the gas migration process in the shale containing micro-cracks is of low permeability, about within the order of 10^{-3} mD. Figure 13 shows that reservoirs with higher permeability in microfractures can use Darcy's equation to describe the gas flow in shale gas reservoirs. The flow state in shale pores and fissures includes diffusion and slip effects. The stronger the brittleness of shale, the easier it is for the fractures formed in the near-wellbore area to maintain a larger opening under the action of proppant, and the easier it is to form fracture networks that are conducive to shale gas flow; but at the same time, it is also susceptible to mud pollution during the mining process of shale gas, it is necessary to focus on the brittleness index of the shale and the water-rock interaction in order to enhance the gas production in the early and later exploiting stages (Florence et al., 2007; Perera et al., 2011; Ghanizadeh et al., 2014; Ghanizadeh et al., 2014; Yin et al., 2015; Wu et al., 2017; Hu et al., 2018; Liu et al., 2018; Zhang and Wang, 2018).

Liquid or supercritical CO_2 is a kind of fracturing fluid worth promoting in the region of southwest China, not only because of the displacement effect of CO_2 on shale gas (Du et al., 2020; Yang et al., 2022), but also due to its potential for controlling injection risk and facilitating carbon dioxide storage. Due to the competitive adsorption of carbon dioxide and methane in shale pores, methane will be displaced by carbon dioxide and flow out of the pores; at the same time, carbon dioxide is stored in the shale reservoir *in situ* (Zhou et al., 2010; Du et al., 2017; Du et al., 2018; Du et al., 2019a; Du et al., 2019b; Du X. D. et al., 2020; Du et al., 2020b; Du et al., 2021; Du et al., 2022). Importantly, the mineral composition of shale plays a crucial role in carbon dioxide sequestration. After shale is exposed to reservoirs fluids, the proportion of quartz and dolomite content increases, and the content of calcite, feldspar minerals and clay minerals decrease. This may be because carbon dioxide dissolves in water to form a carbonic acid solution (Gunter et al., 1993). Most of the silicic acid salt minerals and carbonate minerals in shale will undergo complex chemical reactions with ions such as $H^+/HCO_3^-/CO_3^{2-}$ in an acidic reservoir environment. The comprehensive reaction is expressed as: Clay mineral + feldspar + H_2O + CO_2 ↔ Quartz + calcite + dolomite + kaolinite + siderite. Kaolinite reacts with carbonate minerals to form quartz and dolomite: $[Fe/Mg]5Al_2Si_3O_{10}(OH)_8 + 5CaCO_3 + 5CO_2 \leftrightarrow 5Ca[Fe/Mg](CO_3)_2 + Al_2Si_2O_5(OH)_4 + SiO_2 + 2H_2O$. Carbonate rocks such as calcite and dolomite will undergo the following chemical reactions in acidic solutions (Xian et al., 2018; 2019; Zhu et al.,

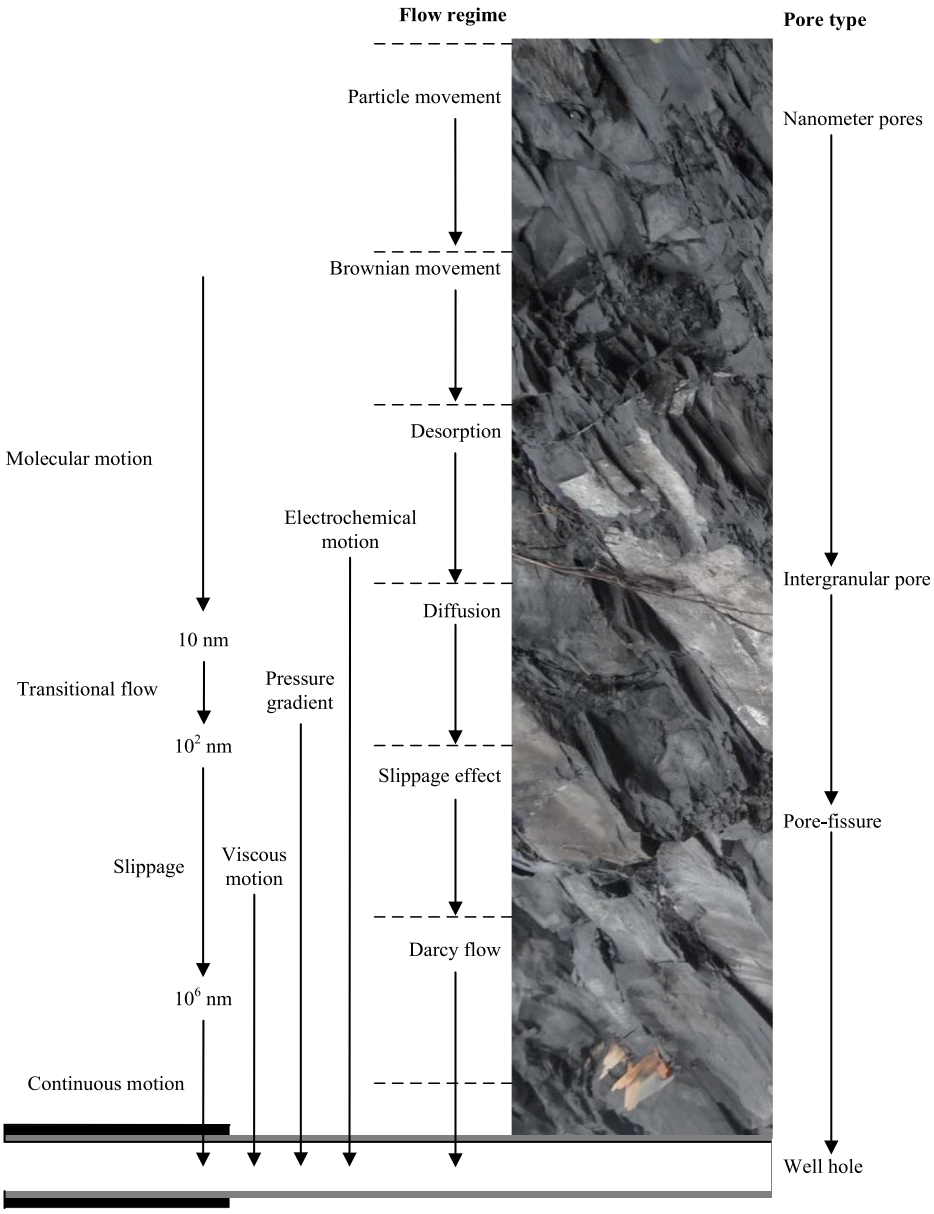

FIGURE 13
Pore type and corresponding flow regime of shale reservoir in gas production, adapted from Javadpour's study (Javadpour, 2009).

2018): $CaCO_3 + H_2O + CO_2 \leftrightarrow Ca^{2+} + 2HCO_3^-$. It can be seen from the reaction formulas that when carbon dioxide and pyrite are dissolved in water, the solution becomes acidic, which promotes the reactions. Clay minerals undergo dissolution and their content decreases. Calcite, dolomite, and other carbonate minerals undergo both dissolution and precipitation. Varied mineral compositions can influence the adsorption, migration, and storage efficiency of CO_2, thereby impacting CO_2 sequestration outcomes. Certain shale minerals, such as clay minerals and iron oxides, have the capacity to adsorb CO_2 by offering sites on their surfaces, thus facilitating CO_2 storage. Conversely, specific carbonate minerals may react with CO_2 to form carbonates, effectively trapping CO_2 within the shale strata permanently. When the solubility of carbon dioxide in the fluid reaches saturation, the chemical reactions go to a balance; in addition, the carbon dioxide absorbed in the shale pores, cracks, and fractures as the adsorption property of carbon dioxide in shale pores is stronger than that of methane, showing competitive adsorption characteristics. And finally, the carbon dioxide can be trapped in the shale reservoirs. Furthermore, the mineral composition can affect the diffusion and migration of CO_2. Some minerals may alter the diffusion rate of CO_2 or obstruct CO_2 migration pathways, thereby affecting the efficiency of CO_2 sequestration. Therefore, comprehending the mineral composition of shale is imperative for assessing the feasibility and effectiveness of CO_2 sequestration.

In the shale gas development region of southwest China, there has been mounting concern among local residents regarding the correlation between the region's increased seismic activity and shale gas extraction activities. These concerns were amplified when

an earthquake struck Jiaoshiba area of Fuling, Chongqing on 7 February 2017, leaving residents in a state of panic because the area was a pilot area for shale gas extraction. Recent studies have demonstrated that water injection fracturing and wastewater treatment can trigger earthquakes during shale gas extraction (Ellsworth, 2013; Bao and Eaton, 2016; Elsworth et al., 2016). Moreover, these microearthquakes have a significant lagging effect on shale gas extraction in the region (Tang et al., 2018). The process of water injection during oil and gas or geothermal energy development has been identified as a potential trigger for seismic activity, as it can lubricate faults, thereby reactivating them and inducing earthquakes (Dou et al., 2020a; Dou et al., 2020b; Shang et al., 2020). Statistics show a notable surge in earthquake frequency across the central and eastern United States following the intensification of shale gas development (van der Baan and Calixto, 2017; Canales et al., 2022). In regions and during periods with a lot of shale gas development activities, the frequency of earthquakes is significantly higher than that of other regions. For instance, between 2010 and 2012, nearly 300 earthquakes larger than magnitude 3 occurred in the central and eastern parts of the United States. However, current research shows that mining-induced earthquakes tend to be of minor magnitude and localized, occurring predominantly in shallow areas. Besides, these small earthquakes can also facilitate the release of tectonic stress within the formations without causing earthquakes of greater magnitude, and may cause secondary engineering disaster risk (Li et al., 2023).

At present, the research of scientists is insufficient to fully elucidate the geophysical change process and seismic mechanism behind induced earthquakes. For example, the fluid pressurization rate plays a crucial role in triggering seismicity during the injection of hydraulic fracturing in deep gas shale formations (Wang X. Y. et al., 2023). The more brittle the shale rock, the greater the strain energy released during rupture. The brittleness index of shale that is focused on in this study reflects this brittle-ductile characteristics of shale. Therefore, future research in shale gas development in southwest China should focus on clarifying the interplay between development activities and induced earthquakes, as well as understanding the interaction and influence law between earthquake occurrence and development and exploitation activities, especially hydraulic fracturing. Additionally, from the perspective of the rheology of rock mass, the memory mechanism of casing deformation and wellbore instability during development should also be investigated. In the future, the characterization of the physical and mechanical parameters of shale should prioritize the development of "high-fidelity" *in-situ* fidelity sampling processes, fidelity transfer technical measures, fidelity testing methods and technologies, to obtain "high-fidelity" physical and mechanical characteristics and parameters that closely mirror *in-situ* formation conditions.

6 Conclusion

The shale gas exploitation in China not only serves to meet the constantly increasing demand for natural gas in China but also represents a promising frontier for energy supply all over the world. This study focuses on elucidating the fundamental physical and mechanical properties of Longmaxi shale outcrop samples from the favorable block of gas shale in Changning, Sichuan, located in southwest China. It delves into the influence of these physical and mechanical characteristics and minerals composition on brittleness. Furthermore, it provides corresponding recommendations for the development and risk control during shale gas exploitation. The conclusions of the study are outlined as follows.

1) The *TOC* content of shale in Changning area is high, ranging from 4.14% to 4.26%. The main minerals in shale specimens include quartz and clay, and most of them also contain calcite, dolomite, and other minerals. Shale mainly contains Si, C, CA, Al, Fe, K, Mg, and S, as well as some trace elements. 2) The pores of shale are widely distributed. Low-temperature N_2 adsorption test demonstrates that the pores of shale are mainly slit pores. The results of SEM reveal diverse pore types, mainly including intergranular pores, mineral particle dissolution pores, and internal pores of organic matter. Nuclear magnetic resonance core micro nondestructive testing imaging and analysis shows that the pore size of the experimental shale core predominantly falls within the range of 5–237 nm, with medium to large pores dominating; the pores are mainly of a nano-pore structure; and it is a rock of ultra-low permeability reservoir. 3) Under the confining stress of 0–55 MPa, with the increase of confining stress, the peak strength and peak strain of shale gradually increase with the increase of confining stress, and the peak strength is positive to the confining stress. Correlation, however, the peak strain increase rate gradually slows down, and there is a threshold. 4) A universal brittleness index considering the influence of water state and the mechanical parameter is proposed, and the influence of the composition of various minerals in this brittleness index can more truly reflect the brittleness index of deep formation. Thus, the "high-fidelity" sampling becomes increasingly paramount for shale exploration under *in-situ* conditions. It is necessary to focus on the brittleness index of the shale and the water-rock interaction to enhance the gas production in the early and later exploiting stages.

Data availability statement

The original contributions presented in the study are included in the article/Supplementary Material, further inquiries can be directed to the corresponding author.

Author contributions

GL: Data curation, Funding acquisition, Investigation, Methodology, Resources, Writing–original draft. DS: Data curation, Funding acquisition, Investigation, Supervision, Visualization, Writing–review and editing. YZ: Data curation, Formal Analysis, Investigation, Validation, Writing–original draft. XD: Conceptualization, Funding acquisition, Investigation, Methodology, Validation, Writing–original draft.

Funding

The author(s) declare that financial support was received for the research, authorship, and/or publication of this article. This work was supported by Natural Science Foundation of Hunan Province (No. 2021JJ40028), Yunnan Provincial Department of Education Science Research Fund Project (No. 2022J0055), Yunnan Fundamental Research Projects (Nos 202101BE070001-039 and 202401AT070406), and Yunnan Province "Xingdian Talent Support Program" Youth Talent Special Project (No. XDYC-QNRC-2022-0595).

Conflict of interest

Author YZ was employed by the Sinohydro Bureau 8 Co., Ltd.

The remaining authors declare that the research was conducted in the absence of any commercial or financial relationships that could be construed as a potential conflict of interest.

Publisher's note

All claims expressed in this article are solely those of the authors and do not necessarily represent those of their affiliated organizations, or those of the publisher, the editors and the reviewers. Any product that may be evaluated in this article, or claim that may be made by its manufacturer, is not guaranteed or endorsed by the publisher.

References

Bai, S., Cheng, D., Wan, J., Yang, L., Peng, H., Guo, X., et al. (2016). Quantitative characterization of sandstone NMR T2 spectrum. 37, 382–391. doi:10.7623/syxb201603010

Bao, X. W., and Eaton, D. W. (2016). Fault activation by hydraulic fracturing in western Canada. *Science* 354 (6318), 1406–1409. doi:10.1126/science.aag2583

Barham, A., Ismail, M. S., Hermana, M., Padmanabhan, E., Baashar, Y., and Sabir, O. (2021). Predicting the maturity and organic richness using artificial neural networks (ANNs): a case study of Montney Formation, NE British Columbia, Canada. *Alexandria Eng. J.* 60 (3), 3253–3264. doi:10.1016/j.aej.2021.01.036

Bishop, A. W. (1967). Progressive failure-with special reference to the mechanism causing it. *Proc. Geotech. Conf.* 2, 142–150.

Canales, M. R., Rodriguez-Pradilla, G., Yusifbayov, J., and van der Baan, M. (2022). The rise, peak and decline of the seismic hazard related to hydraulic fracturing activities in the duvernay play, fox creek area, alberta. *J. Geophys. Research-Solid Earth* 127 (1). e2021JB023060. doi:10.1029/2021jb023060

Chen, J., and Xiao, X.-M. (2013). Mineral composition and brittleness of three sets of Paleozoic organic-rich shales in China South area. *J. China Coal Soc.* 38, 822–826. doi:10.13225/j.cnki.jccs.2013.05.018

Chen, L., Jiang, Z. X., Liu, K. Y., Tan, J. Q., Gao, F. L., and Wang, P. F. (2017). Pore structure characterization for organic-rich Lower Silurian shale in the Upper Yangtze Platform, South China: a possible mechanism for pore development. *J. Nat. Gas Sci. Eng.* 46, 1–15. doi:10.1016/j.jngse.2017.07.009

Chen, S., Shuai, Q., Gao, Q., Tian, Y., Xu, S., and Huang, Y. (2015a). Analysis of the pore structure of shale in Ordos Basin by SEM with Nitrogen gas adsorption-Desorption. *Rock Mineral Analysis* 34 (6), 636–642. doi:10.15898/j.cnki.11-2131/td.2015.06.006

Chen, S., Zhu, Y., Wang, H., Liu, H., Wei, W., and Fang, J. (2011). Characteristics and significance of mineral compositions of Lower Silurian Longmaxi Formation shale gas reservoir in the southern margin of Sichuan Basin. *Shiyou Xuebao/Acta Pet. Sin.* 32 (5), 775–782.

Chen, Y. Y., Wei, L., Mastalerz, M., and Schimmelmann, A. (2015b). The effect of analytical particle size on gas adsorption porosimetry of shale. *Int. J. Coal Geol.* 138, 103–112. doi:10.1016/j.coal.2014.12.012

Cheng, H., Wei, J., and Cheng, Z. (2022). Study on sedimentary facies and reservoir characteristics of Paleogene sandstone in Yingmaili block, Tarim basin. *Geofluids* 2022, 1–14. doi:10.1155/2022/1445395

Dai, J., Zou, C., Dong, D., Ni, Y., Wu, W., Gong, D., et al. (2016). Geochemical characteristics of marine and terrestrial shale gas in China. *Mar. Petroleum Geol.* 76, 444–463. doi:10.1016/j.marpetgeo.2016.04.027

Deng, Y., Wang, W., Su, Y., Sun, S., and Zhuang, X. (2023). An unsupervised machine learning based double sweet spots classification and evaluation method for tight reservoirs. *J. Energy Resour. Technol.* 145 (7). doi:10.1115/1.4056727

Diao, H. (2013). Rock mechanical properties and brittleness evaluation of shale reservoir. *Acta Petrol. Sin.* 29 (9), 3300–3306. (in Chinese). doi:10.3969/j.issn.1001-0890.2012.04.004

Dou, Z., Gao, T., Zhao, Z., Li, J., Yang, Q., and Shang, D. (2020a). The role of water lubrication in critical state fault slip. *Eng. Geol.*, 271, 105606. doi:10.1016/j.enggeo.2020.105606

Dou, Z., Shang, D., Zhao, Z., Gao, T., Li, J., and Yang, Q. (2020b). "Experimental study on water injection induced fault slip under critical state," in 14th International Congress on Rock Mechanics and Rock Engineering, ISRM, Spa Resort, Brazil, September, 2020, 1410–1416.

Du, X. D., Cheng, Y. G., Liu, Z. J., Hou, Z. K., Wu, T. F., Lei, R. D., et al. (2020). Study on the adsorption of CH_4, CO_2 and various $CH_{4/CO}2$ mixture gases on shale. *Alexandria Eng. J.* 59 (6), 5165–5178. doi:10.1016/j.aej.2020.09.046

Du, X. D., Cheng, Y. G., Liu, Z. J., Hou, Z. K., Wu, T. F., Lei, R. D., et al. (2020b). Study on the adsorption of CH_4, CO_2 and various CH_4/CO_2 mixture gases on shale. *Alexandria Eng. J.* 59, 5165–5178. doi:10.1016/j.aej.2020.09.046

Du, X. D., Gu, M., Duan, S., and Xian, X. F. (2017). Investigation of CO_2-CH_4 displacement and transport in shale for enhanced shale gas recovery and CO_2 sequestration. *J. Energy Resour. Technology-Transactions ASME* 139, 1–9. doi:10.1115/1.4035148

Du, X. D., Gu, M., Duan, S., and Xian, X. F. (2018). The influences of CO_2 injection pressure on CO_2 dispersion and the mechanism of CO_2-CH_4 displacement in shale. *J. Energy Resour. Technology-Transactions ASME* 140. 012907-1-012907-9. doi:10.1115/1.4037687

Du, X. D., Gu, M., Hou, Z. K., Liu, Z. J., and Wu, T. F. (2019a). Experimental study on the kinetics of adsorption of CO_2 and CH_4 in gas-bearing shale reservoirs. *Energy & Fuels* 33, 12587–12600. doi:10.1021/acs.energyfuels.9b03176

Du, X. D., Gu, M., Liu, Z. J., Zhao, Y., Sun, F. L., and Wu, T. F. (2019b). Enhanced shale gas recovery by the injections of CO_2, N_2, and CO_2/N_2 mixture gases. *Energy & Fuels* 33, 5091–5101. doi:10.1021/acs.energyfuels.9b00822

Du, X. D., Guang, W. F., Cheng, Y. G., Hou, Z. K., Liu, Z. J., Yin, H., et al. (2020a). Thermodynamics analysis of the adsorption of CH_4 and CO_2 on montmorillonite. *Appl. Clay Sci.* 192, 105631. doi:10.1016/j.clay.2020.105631

Du, X. D., Pang, D. D., Cheng, Y. G., Zhao, Y., Hou, Z. K., Liu, Z. J., et al. (2021). Adsorption of CH_4, N_2, CO_2 and their mixture on montmorillonite with implications for enhanced hydrocarbon extraction by gas injection. *Appl. Clay Sci.* 210, 106160. doi:10.1016/j.clay.2021.106160

Du, X. D., Pang, D. D., Zhao, Y., Hou, Z. K., Wang, H. L., and Cheng, Y. G. (2022). Investigation into the adsorption of CO_2, N_2 and CH_4 on kaolinite clay. *Arabian J. Chem.* 15, 103665. doi:10.1016/j.arabjc.2021.103665

Ellsworth, W. L. (2013). Injection-induced earthquakes. *Science* 341 (6142), 1225942. doi:10.1126/science.1225942

Elsworth, D., Spiers, C. J., and Niemeijer, A. R. (2016). Understanding induced seismicity. *Science* 354 (6318), 1380–1381. doi:10.1126/science.aal2584

Estrada, J. M., and Bhamidimarri, R. (2016). A review of the issues and treatment options for wastewater from shale gas extraction by hydraulic fracturing. *Fuel* 182, 292–303. doi:10.1016/j.fuel.2016.05.051

Fan, R., Liao, G., Mao, R., Luo, X., Hou, L., Zhang, H., et al. (2023). Nuclear magnetic resonance response characteristics and quantitative evaluation method of fluid saturation of lacustrine shale oil. *Front. Earth Sci.* 11. doi:10.3389/feart.2023.1117193

Felix, V., Jannot, Y., and Degiovanni, A. (2012). A thermal porosimetry method to estimate pore size distribution in highly porous insulating materials. *Rev. Sci. Instrum.* 83 (5), 054903. doi:10.1063/1.4704842

Florence, F., Rushing, J., Newsham, K., and Blasingame, T. (2007). Improved permeability prediction relations for low permeability sands. *Proc. Rocky Mt. Oil Gas Technol. Symposium*. doi:10.2523/107954-ms

Gao, J., Li, X., Cheng, G., Luo, H., and Zhu, H. (2023). Structural evolution and characterization of organic-rich shale from macroscopic to microscopic

resolution: the significance of tectonic activity. *Adv. Geo-Energy Res.* 10 (2), 84–90. doi:10.46690/ager.2023.11.03

Gao, Z. Y., and Hu, Q. H. (2018). Pore structure and spontaneous imbibition characteristics of marine and continental shales in China. *AAPG Bull.* 102 (10), 1941–1961. doi:10.1306/03291817297

Ghanizadeh, A., Amann-Hildenbrand, A., Gasparik, M., Gensterblum, Y., Krooss, B. M., and Littke, R. (2014). Experimental study of fluid transport processes in the matrix system of the European organic-rich shales: II. Posidonia Shale (Lower Toarcian, northern Germany). *Int. J. Coal Geol.* 123, 20–33. doi:10.1016/j.coal.2013.06.009

Goodway, B., Perez, M., Varsek, J., and Abaco, C. (2010). Seismic petrophysics and isotropic-anisotropic AVO methods for unconventional gas exploration. *Lead. Edge* 29 (12), 1 500–501 508. doi:10.1190/1.3525367

Gunter, W. D., Perkins, E. H., and Mccann, T. J. (1993). Aquifer disposal of CO_2 -rich gases: reaction design for added capacity. *Energy Convers. Manag.* 34 (9–11), 941–948. doi:10.1016/0196-8904(93)90040-H

Hackley, P. C., and Lünsdorf, N. K. (2018). Application of Raman spectroscopy as thermal maturity probe in shale petroleum systems: insights from natural and artificial maturation series. *Energy & Fuels* 32 (11), 11190–11202. doi:10.1021/acs.energyfuels.8b02171

Hou, Z.-K., Cheng, H.-L., Sun, S.-W., Chen, J., Qi, D.-Q., and Liu, Z.-B. (2019). Crack propagation and hydraulic fracturing in different lithologies. *Appl. Geophys.* 16 (2), 243–251. doi:10.1007/s11770-019-0764-3

Hu, J. G., Tang, S. H., and Zhang, S. H. (2016). Investigation of pore structure and fractal characteristics of the lower silurian Longmaxi shales in western hunan and hubei provinces in China. *J. Nat. Gas Sci. Eng.* 28, 522–535. doi:10.1016/j.jngse.2015.12.024

Hu, Q. H., Liu, X. G., Gao, Z. Y., Liu, S. G., Zhou, W., and Hu, W. X. (2015). Pore structure and tracer migration behavior of typical American and Chinese shales. *Petroleum Sci.* 12 (4), 651–663. doi:10.1007/s12182-015-0051-8

Hu, Y., Gan, Q., Hurst, A., and Elsworth, D. (2018). Evolution of permeability in sand injectite systems. *Int. J. Rock Mech. Min. Sci.* 106, 176–189. doi:10.1016/j.ijrmms.2018.04.018

Hucka, V., and Das, B. (1974). Brittleness determination of rocks by different methods. *Int. J. Rock Mech. Min. Sci. Geomechanics Abstr.*, 11(10), 389–392. doi:10.1016/0148-9062(74)91109-7

Jannot, Y., Degiovanni, A., and Camus, M. (2018). Extension of the thermal porosimetry method to high gas pressure for nanoporosimetry estimation. *Rev. Sci. Instrum.* 89 (4), 044904. doi:10.1063/1.5020117

Jarvie, D. M., Hill, R. J., Ruble, T. E., and Pollastro, R. M. (2007). Unconventional shale gas systems: the Mississippian Barnett Shale of north central Texas as one model for thermogenic shale-gas assessment. *AAPG Bull.* 91 (4), 475–499. doi:10.1306/12190606068

Javadpour, F. (2009). Nanopores and apparent permeability of gas flow in mudrocks (shales and siltstone). *J. Can. Petroleum Technol.* 48, 16–21. doi:10.2118/09-08-16-DA

Ji, L., Qiu, J., Xia, Y., and Zhang, T. (2012). Micro-pore characteristics and methane adsorption properties of common clay minerals by electron microscope scanning. *Acta Pet. Sin.* 33 (2), 249–256.

Jin, X. C., Shah, S. N., Roegiers, J. C., and Zhang, B. (2014). "Fracability evaluation in shale reservoirs-an integrated petrophysics and geomechanics approach," in SPE Hydraulic Fracturing Technology Conference, The Woodlands, Texas, USA, February, 2014. doi:10.2118/168589-MS

Kennedy, M. J., Pevear, D. R., and Hill, R. J. (2002). Mineral surface control of organic carbon in black shale. *Science* 295 (5555), 657–660. doi:10.1126/SCIENCE.1066611

Kim, C., Jang, H., and Lee, J. (2015). Experimental investigation on the characteristics of gas diffusion in shale gas reservoir using porosity and permeability of nanopore scale. *J. Petroleum Sci. Eng.* 133, 226–237. doi:10.1016/j.petrol.2015.06.008

Li, J. (2013). Analysis on mineral components and frangibility of shales in Dongying depression. *Acta Sedimentol. Sin.* 31 (4), 616–620. (in Chinese). doi:10.14027/j.cnki.cjxb.2013.04.008

Li, S., Kuang, Z., and Qiu, S. (2022a). Review of rock brittleness evaluation methods and discussion on their adaptabilities. *J. Eng. Geol.* 30 (1), 59–70. (in Chinese). doi:10.13544/j.cnki.jeg.2021-0677

Li, W. B., Lu, S. F., Li, J. Q., Zhang, P. F., Chen, C., and Wang, S. Y. (2019b). The coupling relationship between material composition and pore microstructure of southern China marine shale. *Nat. Gas. Geosci.* 30 (1), 27–38. doi:10.11764/j.issn.1672-1926.2018.10.001

Li, X., Li, Q., Wang, Y., Liu, W., Hou, D., Zheng, W., et al. (2023). Experimental study on instability mechanism and critical intensity of rainfall of high-steep rock slopes under unsaturated conditions. *Int. J. Min. Sci. Technol.*, 33(10), 1243–1260. doi:10.1016/j.ijmst.2023.07.009

Li, Y., Yang, J., Chen, J., Ma, X., and Cai, J. (2022b). "*In situ* stress and mechanical properties of unconventional gas reservoirs," in *Sustainable natural gas reservoir and production engineering* (Houston, Texas: Gulf Professional Publishing), 83–106. doi:10.1016/B978-0-12-824495-1.00012-7

Li, B., Cui, C., Zhang, Y., Hu, B., and Luo, Q. (2019a). Analysis of shale gas accumulation conditions in niutitang formation of lower cambrian in baojing area of hunan Province. *Geol. Surv. China* (3), 22–28. doi:10.19388/j.zgdzdc.2019.03.03

Liu, G. (2017). *Supercritical CO_2 fracturing of shale and its permeability variation under multi-field coupling conditions*. Ph.D. thesis. Chongqing: Chongqing University.

Liu, G., Shang, D., Chu, P., Lu, J., Li, J., and Zhao, Y. (2024). Thermomechanical coupling seepage in fractured shale under stimulation of supercritical carbon dioxide. *Front. Earth Sci.* 12, 1399806. doi:10.3389/feart.2024.1399806

Liu, G., Xian, X., Zhou, J., Zhao, Y., Yin, H., Guo, Y., et al. (2017a). Dynamic permeability change of supercritical CO_2 fractured shale and its influencing factors. *Meitan Xuebao/Journal China Coal Soc.* 42 (10), 2670–2678. doi:10.13225/j.cnki.jccs.2017.0262

Liu, G. J., Xian, X. F., Ping, Z., Zhang, L., Liu, Q. L., and Zhang, S. (2016a). Experimental study the impact of loading deformation characteristics and mineral composition on shale rock brittleness. 41, 369–375. doi:10.13225/j.cnki.jccs.2015.1746

Liu, G.-J., Xian, X.-F., Zhou, J.-P., Zhang, L., Liu, Q.-L., and Zhang, S.-W. (2016b). Experimental study the impact of loading deformation characteristics and mineral composition on shale rock brittleness. *Meitan Xuebao/Journal China Coal Soc.* 41, 369–375. doi:10.13225/j.cnki.jccs.2015.1746

Liu, G.-J., Xian, X.-F., Zhou, J.-P., Zhang, L., Liu, Q.-L., Zhao, Y., et al. (2017b). Experimental study on the supercritical CO_2 fracturing of shale. *Meitan Xuebao/Journal China Coal Soc.* 42 (3), 694–701. doi:10.13225/j.cnki.jccs.2016.0604

Liu, S., Li, H., and Zhang, Y. (2015). Analysis of TOC content influence on shale brittleness index evaluation. *Well Logging Technol.* 39 (3), 352–356.

Liu, Y., Li, M., Yin, G., Zhang, D., and Deng, B. (2018). Permeability evolution of anthracite coal considering true triaxial stress conditions and structural anisotropy. *J. Nat. Gas Sci. Eng.* 52, 492–506. doi:10.1016/j.jngse.2018.02.014

Maex, K., Baklanov, M. R., Shamiryan, D., Iacopi, F., Brongersma, S. H., and Yanovitskaya, Z. S. (2003). Low dielectric constant materials for microelectronics. *J. Appl. Phys.* 93 (11), 8793–8841. doi:10.1063/1.1567460

Matthews, H. L., Schein, G., and Malone, M. (2007). "Stimulation of gas shales: they're all the same-right? College Station," in SPE Hydraulic Fracturing Technology Conference, Texas, USA. doi:10.2118/106070-MS

Montgomery, S. L., Jarvie, D. M., Bowker, K. A., and Pollastro, R. M. (2005). Mississippian Barnett Shale, Fort Worth basin, north-central Texas: gas-shale play with multi-trillion cubic foot potential. *AAPG Bull.* 89 (2), 155–175. doi:10.1306/09170404042

Nelson, R. A. (2001). *Geologic analysis of naturally fractured reservoirs*. Houston, USA: Gulf Professional Publishing.

Ning, C., Jiang, Z., Gao, Z., Su, S., Li, T., Wang, G., et al. (2017). Characteristics and controlling factors of reservoir space of mudstone and shale in Es3x in the Zhanhua Sag. *Mar. Petroleum Geol.* 88, 214–224. doi:10.1016/j.marpetgeo.2017.08.025

Perera, M. S. A., Ranjith, P. G., Choi, S. K., and Airey, D. (2011). The effects of sub-critical and super-critical carbon dioxide adsorption-induced coal matrix swelling on the permeability of naturally fractured black coal. *Energy* 36 (11), 6442–6450. doi:10.1016/j.energy.2011.09.023

Rickman, R., Mullen, M., Petre, E., Grieser, B., and Kundert, D. (2008). *A practical use of shale petrophysics for stimulation design optimization: all shale plays are not clones of the Barnett Shale*. Denver, Colorado, USA: SPE Annual Technical Conference and Exhibition. doi:10.2118/115258-MS

Ross, D. J. K., and Bustin, R. M. (2009). The importance of shale composition and pore structure upon gas storage potential of shale gas reservoirs. *Mar. Petroleum Geol.* 26 (6), 916–927. doi:10.1016/j.marpetgeo.2008.06.004

Shang, D., Zhao, Z., Dou, Z., and Yang, Q. (2020). Shear behaviors of granite fractures immersed in chemical solutions. *Eng. Geol.*, 279, 105869. doi:10.1016/j.enggeo.2020.105869

Su, S., and Zou, Z. (2016). Characterization methods of freeze-thaw nuclear magnetic resonance measurement of shale gas reservoir nano-pore. *Resour. Environ. Eng.* 30 (1), 66. doi:10.16536/j.cnki.issn.1671-1211.201601011

Tang, M., Li, C., Wang, X., Wang, Z., Yang, Y., Shu, T., et al. (2018). 重庆涪陵焦石坝页岩气开采诱发地震加密观测 (translated title: intensive observation of shale gas production induced earthquake in Jiaoshiba, Fuling, Chongqing). *Recent Dev. World Seismol.* 8, 139–140. doi:10.3969/j.issn.0253-4975.2018.08.121

Tang, Y., Tang, X., Wang, G.-y., and Zhang, Q. (2011). Summary of hydraulic fracturing technology in shale gas development. *Geol. Bull. China* 30 (0203), 393–399.

Tian, H., Zhang, S., Liu, S., and Zhang, H. (2012). Determination of organic-rich shale pore features by mercury injection and gas adsorption methods. *Acta Pet. Sin.* 33 (3), 419–427.

van der Baan, M., and Calixto, F. J. (2017). Human-induced seismicity and large-scale hydrocarbon production in the USA and Canada. *Geochem. Geophys. Geosystems* 18 (7), 2467–2485. doi:10.1002/2017gc006915

Wang, F. P., and Gale, J. F. W. (2009). Screening criteria for shale gas systems. *Gulf Coast Assoc. Geol. Soc. Transcations* 59, 779–793.

Wang, H. Y., Liu, Y. Z., Dong, D. Z., Zhao, Q., and Du, D. (2013). Scientific issues on effective development of marine shale gas in southern China. *Petroleum Explor. Dev.* 40 (5), 615–620. doi:10.1016/s1876-3804(13)60080-4

Wang, W., Yu, W., Wang, S., Zhang, L., Zhang, Q., and Su, Y. (2023a). Mitigating interwell fracturing interference: numerical investigation of parent well depletion affecting infill well stimulation. *J. Energy Resour. Technol.* 146 (1). doi:10.1115/1.4063490

Wang, X. Y., Liu, D. Z., Li, X., and Gao, Q. C. (2023b). Mechanism and implications of shut-in induced earthquakes. *Alexandria Eng. J.* 65, 837–846. doi:10.1016/j.aej.2022.09.042

Wang, Y., Dong, D., Li, J., Wang, S., Li, X., Wang, L., et al. (2012). Reservoir characteristics of shale gas in Longmaxi Formation of the lower silurian, southern sichuan. *Shiyou Xuebao/Acta Pet. Sin.* 33 (4), 551–561.

Wang, Z., Chen, L., Chen, D., Lai, J., Deng, G., Liu, Z., et al. (2020). Characterization and evaluation of shale lithofacies within the lowermost longmaxi-wufeng formation in the southeast Sichuan basin. *J. Petroleum Sci. Eng.* 193, 107353. doi:10.1016/j.petrol.2020.107353

Wei, X. F., Liu, R. B., Zhang, T. S., and Liang, X. (2013). Micro-pores structure characteristics and development control factors of shale gas reservoir: a case of Longmaxi Formation in XX area of southern Sichuan and northern Guizhou [Article]. *Nat. Gas. Geosci.* 24 (5), 1048–1059. doi:10.11764/j.issn.1672-1926.2013.05.1048

Wei, Z. Z., Zhu, S. Y., and Li, C. (2021). A novel aluminum-based shale inhibitor and its wellbore stabilization effect. *Alexandria Eng. J.* 60 (6), 5463–5471. doi:10.1016/j.aej.2021.04.009

Wu, W., Reece, J. S., Gensterblum, Y., and Zoback, M. D. (2017). Permeability evolution of slowly slipping faults in shale reservoirs. *Geophys. Res. Lett.* 44 (22), 11368–11375. doi:10.1002/2017GL075506

Xian, H. Y., Du, R. X., Zhu, J. X., Chen, M., Tan, W., Zhu, R. L., et al. (2018). Hydration induced bandgap shift at pyrite-water interface. *Appl. Phys. Lett.* 113, 123901. doi:10.1063/1.5048542

Xian, H. Y., Zhu, J. X., Tan, W., Tang, H. M., Liu, P., Zhu, R. L., et al. (2019). The mechanism of defect induced hydroxylation on pyrite surfaces and implications for hydroxyl radical generation in prebiotic chemistry. *Geochimica Cosmochimica Acta* 244, 163–172. doi:10.1016/j.gca.2018.10.009

Xie, C., Nguyen, H., Choi, Y., and Armaghani, D. J. (2022). Optimized functional linked neural network for predicting diaphragm wall deflection induced by braced excavations in clays. *Geosci. Front.* 13 (2), 101313. doi:10.1016/j.gsf.2021.101313

Xie, R. (2007). *Structural geology*. Xuzhou: China University of Mining and Technology.

Yang, F., Ning, Z., Zhang, S., Hu, C., Du, L., and Liu, H. (2013). Characterization of pore structures in shales through nitrogen adsorption experiment. *Nat. Gas. Ind.* 33 (4), 135–140. doi:10.3787/j.issn.1000-0976.2013.04.025

Yang, H., Zhao, Y., Zhang, X., Liu, G., Du, X., Shang, D., et al. (2022). Supercritical CO_2 fracturing with different drilling depths in shale. *Energy Sources, Part A Recovery, Util. Environ. Eff.* 44 (4), 10603–10622. doi:10.1080/15567036.2019.1673850

Yang, R., He, S., Hu, Q. H., Hu, D. F., Zhang, S. W., and Yi, J. Z. (2016a). Pore characterization and methane sorption capacity of over-mature organic-rich Wufeng and Longmaxi shales in the southeast Sichuan Basin, China. *Mar. Petroleum Geol.* 77, 247–261. doi:10.1016/j.marpetgeo.2016.06.001

Yang, R., He, S., Yi, J. Z., and Hu, Q. H. (2016b). Nano-scale pore structure and fractal dimension of organic-rich Wufeng-Longmaxi shale from Jiaoshiba area, Sichuan Basin: investigations using FE-SEM, gas adsorption and helium pycnometry. *Mar. Petroleum Geol.* 70, 27–45. doi:10.1016/j.marpetgeo.2015.11.019

Yang, Y., Teng, G., Zhu, D., Zhang, J., Cao, G., Zhang, H., et al. (2021). Investigation of the evolution of pore structure of Longmaxi shale in south China. *Geochimica* 50 (04), 415–428. doi:10.19700/j.0379-1726.2021.04.007

Yin, G., Li, M., Wang, J. G., Xu, J., and Li, W. (2015). Mechanical behavior and permeability evolution of gas infiltrated coals during protective layer mining. *Int. J. Rock Mech. Min. Sci.* 80, 292–301. doi:10.1016/j.ijrmms.2015.08.022

Yuan, Y. J., Rezaee, R., Verrall, M., Hu, S. Y., Zou, J., and Testmanti, N. (2018). Pore characterization and clay bound water assessment in shale with a combination of NMR and low-pressure nitrogen gas adsorption. *Int. J. Coal Geol.* 194, 11–21. doi:10.1016/j.coal.2018.05.003

Zhang, C., Wang, Y., Dong, D., Li, X., and Guan, Q. (2016). Evaluation of the Wufeng-Longmaxi shale brittleness and prediction of "sweet spot layers" in the Sichuan Basin. *Nat. Gas. Ind.* 36 (9), 51–60. doi:10.3787/j.issn.1000-0976.2016.09.006

Zhang, L.-W., Li, S.-C., and Sun, Q.-Z. (2006). Experimental research on distributing rule of water content and strength parameter of shale in deep strata. *Yantu Lixue/Rock Soil Mech.* 27 (S1), 511–514.

Zhang, P.-F., Lu, S.-F., Li, J.-Q., Chang, X.-C., Zhang, J.-J., Pang, Y.-M., et al. (2023). Quantitative characterization of shale pore connectivity and controlling factors using spontaneous imbibition combined with nuclear magnetic resonance T2 and T1-T2. *Petroleum Sci.* 20 (4), 1947–1960. doi:10.1016/j.petsci.2023.03.011

Zhang, Q., Liu, Z., Liu, C., Zhu, X., Steel, R. J., Tian, H., et al. (2021). Experimental study on the development characteristics and controlling factors of microscopic organic matter pore and fracture system in shale. *Front Earth Sci.* 9, 773960. doi:10.3389/feart.2021.773960

Zhang, S., Shen, Z., He, Y., Zhu, Z., Ren, Q., and Zhang, L. (2023b). Pore structure alteration of shale with exposure to different fluids: the Longmaxi Formation shale in the Sichuan basin, China. *Minerals* 13, 1387. doi:10.3390/min13111387

Zhang, W., Guo, M., and Jiang, Z. (2011). Parameters and method for shale gas reservoir evaluation. *Nat. Gas. Geosci.* 22 (6), 1093–1099. doi:10.11764/j.issn.1672-1926.2011.06.1093

Zhang, W., and Wang, Q. (2018). Permeability anisotropy and gas slippage of shales from the Sichuan Basin in South China. *Int. J. Coal Geol.* 194, 22–32. doi:10.1016/j.coal.2018.05.004

Zhang, W. M., Meng, G., and Wei, X. (2012a). A review on slip models for gas microflows. *Microfuidics Nanofuidics* 13, 845–882. doi:10.1007/s10404-012-1012-9

Zhang, W. M., Meng, G., and Wei, X. (2012b). A review on slip models for gas microflows. *Microfuidics Nanofuidics* 13, 845–882. doi:10.1007/s10404-012-1012-9

Zhao, L., Mao, W., Liu, Z., and Cheng, S. (2023). Research on the differential tectonic-thermal evolution of Longmaxi shale in the southern Sichuan Basin. *Adv. Geo-Energy Res.* 7 (3), 152–163. doi:10.46690/ager.2023.03.02

Zhou, J., Liu, G., Jiang, Y., Xian, X., Liu, Q., Zhang, D., et al. (2016). Supercritical carbon dioxide fracturing in shale and the coupled effects on the permeability of fractured shale: an experimental study. *J. Nat. Gas Sci. Eng.* 36, 369–377. doi:10.1016/j.jngse.2016.10.005

Zhou, J., Xian, X., Li, X., Jiang, D., and Jiang, Y. (2010). Molecular simulations of the competitive adsorption of carbon dioxide/methane in slit-shape pores. *J. China Coal Soc.* 35 (09), 1512–1517. doi:10.13225/j.cnki.jccs.2010.09.002

Zhu, F., Hu, W., Cao, J., Liu, B., Liu, Y., and Chang, C. (2019). Probe material choice for nuclear magnetic resonance cryoporometry (NMRC) measurements of the nano-scale pore size distribution of unconventional reservoirs. *Energy Explor. Exploitation* 37 (1), 412–428. doi:10.1177/0144598718802475

Zhu, J. X., Xian, H. Y., Lin, X. J., Tang, H. M., Du, R. X., Yang, Y. P., et al. (2018). Surface structure-dependent pyrite oxidation in relatively dry and moist air: implications for the reaction mechanism and sulfur evolution. *Geochimica Cosmochimica Acta* 228, 259–274. doi:10.1016/j.gca.2018.02.050

Zou, C., Dong, D., Wang, S., Li, J., Li, X., Wang, Y., et al. (2010). Geological characteristics and resource potential of shale gas in China. *Petroleum Explor. Dev.* 37 (6), 641–653. doi:10.1016/S1876-3804(11)60001-3

Zou, C., Zhu, R., Bai, B., Yang, Z., Wu, S., Su, L., et al. (2011). First discovery of nano-pore throat in oil and gas reservoir in China and its scientific value. *Acta Petrol. Sin.* 27 (6), 1857–1864.